Geochimica et Cosmochimica Acta Vol. 52, pp. 2573–2598

0016-7037/88/$3.00 + .00

A chemical and isotopic study of hibonite-rich refractory inclusions in primitive meteorites

RICHARD W. HINTON[1,†], ANDREW M. DAVIS[2], DEBRA E. SCATENA-WACHEL[3,‡], LAWRENCE GROSSMAN[1,4] and RONALD J. DRAUS[4]

[1]Enrico Fermi Institute, University of Chicago, Chicago, IL 60637, U.S.A.
[2]James Franck Institute, University of Chicago, Chicago, IL 60637, U.S.A.
[3]Department of Chemistry, University of Chicago, Chicago, IL 60637, U.S.A.
[4]Department of the Geophysical Sciences, University of Chicago, Chicago, IL 60637, U.S.A.

(*Received September* 1, 1987; *accepted in revised form July* 25, 1988)

Abstract—The ion microprobe has been used to determine the concentrations of a number of trace elements (including all 14 stable rare earth elements) and the isotopic compositions of Ca and Mg in seven hibonite-rich refractory inclusions. Hibonite in every inclusion analyzed shows the effect of REE partitioning with other solid or liquid phases, in which hibonite is enriched in light over heavy REE compared to other coexisting phases. This partitioning causes C1 chondrite-normalized enrichments to drop by factors of 4 to 22 from lanthanum to lutetium. Fractionations due to gas-solid partitioning of REE are sometimes superimposed on the pattern produced by partitioning between condensed phases. Two inclusions, HAL and DH-H1, show evidence for formation in extremely oxidizing environments and their Ca is mass fractionated in favor of the heavy isotopes by 7 and 12‰/amu, respectively. Two corundum-hibonite inclusions show evidence of extremely high temperature gas-solid fractionation, such that the more volatile light REE are depleted as a group relative to the more refractory heavy REE. These inclusions both have Ca that is mass fractionated in favor of the light isotopes. Hibonite preserves the largest nuclear isotope anomalies in Ti found to date (FAHEY *et al.*, 1985a; HINTON *et al.*, 1987b), but there does not seem to be a simple relationship between chemical composition, isotopic mass fractionation and the sign and magnitude of nuclear isotopic anomalies in hibonite-rich inclusions. One possibility for producing a variety of chemical compositions and degrees of mass fractionation while preserving nuclear isotope anomalies is by multiple cycles of condensation and evaporation in a turbulent protoplanetary accretion disk (MORFILL, 1983; MORFILL and R. N. CLAYTON, 1986a,b). These cycles could also occur in a presolar nebula with large non-axisymmetric temperature and pressure distributions (BOSS, 1988). Nuclear anomalies are most likely to be preserved in hibonite because hibonite is the most refractory major phase to occur commonly in meteorites.

1. INTRODUCTION

CALCIUM-, ALUMINUM-RICH refractory inclusions in meteorites have attracted considerable attention since the discoveries that they: (1) are composed of very high temperature minerals; (2) are strongly enriched in all refractory trace elements, regardless of geochemical character; (3) contain isotopically anomalous oxygen (R. N. CLAYTON *et al.*, 1973); and (4) contain excess ^{26}Mg which is generally believed to result from the *in situ* decay of short-lived ^{26}Al (GRAY and COMPSTON, 1974; LEE *et al.*, 1976). Refractory inclusions are now known to contain isotopic anomalies in many elements; these anomalies range from simple mass fractionation effects to large excesses or depletions in individual isotopes (nuclear anomalies). These findings demonstrate that the solar nebula was heterogeneous and that freshly synthesized material was added shortly before its collapse. The preservation of large nuclear anomalies in inclusions indicates that material produced in a number of nucleosynthetic processes was incompletely mixed. LATTIMER *et al.* (1977) and D. D. CLAYTON (1978, 1981a) have suggested that differences in isotopic signature and chemistry are to be expected for different nucleosynthetic sources and that these differences in chemistry could influence the distribution and preservation of nuclear anomalies. In D. D. CLAYTON's model, inclusions with large isotopic anomalies should have unusual chemical and mineralogical properties. The petrographic and chemical properties of some refractory inclusions with large isotopic anomalies have been determined, but relationships between mineralogy, chemistry and isotope systematics are unclear (R. N. CLAYTON *et al.*, 1984; NIEDERER *et al.*, 1985; FAHEY *et al.*, 1987a; IRELAND, 1987a,b).

Hibonite is a common minor constituent of refractory inclusions in carbonaceous and ordinary chondrites. While corundum is the first major element-bearing phase to condense in a cooling gas of solar composition, hibonite (ideally $CaAl_{12}O_{19}$) is only slightly less refractory (DAVIS *et al.*, 1982). The crystal structure of corundum does not permit significant substitution of trace elements, while that of hibonite does. Therefore, hibonite is the phase most likely to preserve the chemical and isotopic signature of extremely high temperature processes, such as evaporation and condensation. Corundum and hibonite are the first phases to crystallize from aluminous melts, so hibonite is likely to preserve evidence of the early stages of crystallization of extremely refractory melts. Evidence for the ability of hibonite to record early solar system processes comes from the recent discoveries of very large calcium and titanium isotopic anomalies in this mineral: $\delta^{50}Ti$ values range from −68 to +273‰ (FAHEY *et al.*, 1985a; HINTON *et al.*, 1987b; IRELAND *et al.*, 1988) and $\delta^{48}Ca$ values range from −46 to +105‰ (ZINNER *et al.*, 1986; IRELAND *et al.*, 1988).

Combined isotopic, chemical and petrologic studies require relatively large samples when bulk methods of analysis are used. The only pure hibonite sample that has been analyzed

† *Present address:* Grant Institute of Geology, University of Edinburgh, Edinburgh EH9 3SW, Scotland.

‡ *Present address:* General Electric Corporation, Schenectady, New York 12305.

by these methods was isolated from a unique inclusion containing exceptionally large and pure hibonite grains (LEE *et al.*, 1979, 1980; ALLEN *et al.*, 1980; DAVIS *et al.*, 1982). Hibonite grains in refractory inclusions are usually much smaller and cannot be analyzed by conventional bulk techniques. For such samples, the ion microprobe offers a number of advantages over conventional analytical techniques because of its spatial resolution of 5 to 20 μm. Use of the ion microprobe allows much better integration with other methods now used for chemical and mineralogical studies, because analyses can be made on exactly the same spot previously examined with petrographic and scanning electron microscopes and analyzed with an electron microprobe. Analyses can be made of samples having far greater mineralogical purity than those separated by chemical and physical means for analysis by conventional methods. Recent advances in analytical technique have overcome previous problems due to isobaric molecular interferences, allowing routine determination of many chemical and isotopic properties. Although isotopic analyses made by ion microprobe are at least a factor of ten less precise than those made by thermal ionization mass spectrometry, this is offset by the larger isotopic anomalies seen in smaller inclusions (HUTCHEON *et al.*, 1983; FAHEY *et al.*, 1985a,c, 1986a,b, 1987a; HINTON *et al.*, 1985a, 1987b; IRELAND *et al.*, 1985; ZINNER *et al.*, 1986).

The isotopic compositions of carbon, oxygen, magnesium, silicon, potassium, calcium, titanium, chromium, iron, nickel, strontium, ruthenium, molybdenum, hafnium and lead in meteorite samples have been measured by ion microprobe (R. N. CLAYTON *et al.*, 1984; FAHEY and ZINNER, 1987; FAHEY *et al.*, 1985a, 1986a, 1987a,b,c; HINTON *et al.*, 1984a,b, 1985a,c, 1987a,b; HUTCHEON *et al.*, 1984, 1985, 1987; IRELAND, 1987a,b; IRELAND *et al.*, 1985, 1986, 1988; SCATENA-WACHEL *et al.*, 1984, 1985, 1986; ZINNER and EPSTEIN, 1987; ZINNER *et al.*, 1986, 1987). Rare earth element (REE) and other trace element concentrations can now be determined down to 10 to 50 ppb (this work; FAHEY *et al.*, 1985b, 1987a; HINTON *et al.*, 1985b; ZINNER and CROZAZ, 1986).

This paper combines isotopic and chemical analysis of hibonite grains (and in some cases, coexisting minerals) from carbonaceous and ordinary chondrites in an effort to better understand the chemical processes operating early in the history of the solar system. Most of the inclusions have been analyzed in bulk by INAA and have been petrographically characterized by polarizing microscope, scanning electron microscope (SEM) and electron microprobe methods. Some of the data in this paper have been reported in abstract form (HINTON *et al.*, 1984a, 1985b,c; HINTON and DAVIS, 1986b); in most cases, more analyses have been made to improve precision. Titanium isotopic compositions of a number of these inclusions have been reported by HINTON *et al.* (1987b).

2. SAMPLES

2.1 DJ-1

DJ-1 is an ~100 × 150 μm hibonite crystal obtained by freeze-thaw disaggregation of the Murchison C2 chondrite. It is one of six texturally similar isolated hibonite grains studied by MACPHERSON *et al.* (1983). The titanium isotopic composition of this grain was reported by HINTON *et al.* (1987b).

2.2 MUCH-1

MUCH-1 is a hibonite-rich refractory inclusion of ~300 × 600 μm obtained by excavation from a broken surface of Murchison. Its petrography and mineral chemistry were studied by MACPHERSON *et al.* (1983). Major, minor and trace elements were determined by INAA in hibonite hand-picked from a powder of the bulk inclusion (EKAMBARAM *et al.*, 1984, 1985).

2.3 BB-6

BB-6 is a blue spinel-, hibonite-rich spherule recovered by freeze-thaw disaggregation of Murchison. A small sample of the bulk inclusion was analyzed by INAA (EKAMBARAM *et al.*, 1984, 1985). The petrography was studied by MACPHERSON *et al.* (1983). Magnesium isotopic analyses were given by HUTCHEON *et al.* (1980).

2.4 BB-5

BAR-MATTHEWS *et al.* (1982) studied the petrography, mineral chemistry and magnesium isotopic composition of BB-5, a corundum-hibonite inclusion recovered from Murchison by freeze-thaw disaggregation. The chemistry of BB-5 was studied by EKAMBARAM *et al.* (1984, 1985). The titanium isotopic composition has been measured by HINTON *et al.* (1987b). The isotopic compositions of oxygen, calcium and titanium have also been measured by ZINNER *et al.* (1987) and FAHEY *et al.* (1987c). Six different volumes of BB-5 were sampled by ion microprobe. Two analyses of hibonite-rich areas were made: BB-5-1, on hibonite alone; and BB-5-2, centered on a tiny perovskite grain whose diameter was much smaller than that of the beam spot. Four analyses were made on corundum-rich areas: BB-5-C, on corundum alone; BB-5-O, centered on two trace element-rich phases whose proportions varied as the ion beam sputtered the sample; BB-5-A, centered on a high Lu/Gd trace phase; and BB-5-B, centered on a low Lu/Gd trace phase. There was considerable overlap of the BB-5-2 beam spot onto hibonite and of the BB-5-O, BB-5-A and BB-5-B beam spots onto corundum.

2.5 GR-1

GR-1, a hibonite-corundum inclusion, was obtained by freeze-thaw disaggregation of Murchison. It was described in detail by MACPHERSON *et al.* (1984, 1985), who found two generations of hibonite, an inner magnesium-poor core and an outer magnesium-rich rim, which were separated by corundum. Four spots were analyzed within GR-1. GR-1-C and GR-1-R are analyses of core and rim hibonite, respectively. GR-1-M is an analysis of corundum and GR-1-B is a rastered beam analysis of the entire inclusion. Hibonite in GR-1 is never more than 20 μm across, so there was minor overlap of the GR-1-C and GR-1-R beam spots onto corundum.

2.6 HAL

HAL was found by T. Lee on a broken surface of the Allende C3V carbonaceous chondrite. This isotopically anomalous hibonite-rich inclusion has been extensively studied: its mineralogy and petrography have been described by ALLEN *et al.* (1980); its chemistry by DAVIS *et al.* (1982); its calcium isotopic composition by LEE *et al.* (1979) and HINTON *et al.* (1985c); its magnesium isotopic composition by LEE *et al.* (1979), HINTON and BISCHOFF (1984) and FAHEY *et al.* (1987a); its titanium isotopic composition by FAHEY *et al.* (1987a); and its oxygen isotopic composition by LEE *et al.* (1980).

2.7 DH-H1

DH-H1 is an isolated hibonite fragment found in the Dhajala H3 ordinary chondrite by BISCHOFF and KEIL (1984). The magnesium isotopic composition of DH-H1 was studied by HINTON and BISCHOFF (1984). The main hibonite fragment, 100 × 150 μm (see SEM photomicrograph in HINTON and BISCHOFF, 1984) has a rim of iron-rich spinel (1.5 wt% Cr_2O_3) which pseudomorphically replaced the original hibonite crystal. The spinel was, in turn, replaced by chromite (43 wt% Cr_2O_3). Several small fragments of hibonite are attached to

Table 1. Trace element concentrations, in ppm unless otherwise stated. Ca in hibonite was determined from hibonite stoichiometry, assuming $CaAl_{12}O_{19}$ with substitution of minor elements for Al. Errors due to counting statistics ($\pm 2\sigma$) are given when they exceed 10%.

Sample	Phase	Na	Mg	Si	K	Ca	Sc	Ti	V	Cr	Mn	Fe*	Sr	Y	Zr	Sample
DJ-1	hibonite	4	3075	83	4.9	5.98%	535	7517	24 ±0.2	0.8 ±0.2	0.6	—	64	41	90	DJ-1
MUCH-1	hibonite	27	4643	1889	8.2	5.97%	455	1.01%	34	7.9	15	0.24%	68	76	122	MUCH-1
BB-6	hibonite	73	1.35%	4127	40	5.93%	33.3 ±3.5	2.71%	247	192	132	—	136	≤4.0	51 ±12	BB-6
BB-5-1	hibonite	3.1†	4170†	56	0.21 ±0.04	5.96%	483	9052	53	2.0 ±0.3	0.5 ±0.2	0.68%	75	39	102	BB-5-1
BB-5-2	hibonite + perov.	0.6 ±0.1	4417	120	0.9 ±0.2	5.98%	550	7919	34	1.2 ±0.5	0.5 ±0.4	—	71	76	135	BB-5-2
BB-5-C	corundum	0.3	7.3	93	0.15 ±0.02	125	289	2534	17	0.6 ±0.2	≤0.1	—	0.5	0.6	3.1	BB-5-C
BB-5-O	corundum + 2 unk.	0.1	117	14	0.03 ±0.01	3730	436	3150	23	0.8 ±0.1	0.1	—	—	125	1060	BB-5-O
BB-5-A	corundum + unk. #1	—	8.4	64	—	243	393	2676	—	—	—	—	—	102	1091	BB-5-A
BB-5-B	corundum + unk. #2	—	1794	334	—	2.85%	320	4833	—	—	—	—	—	96	74	BB-5-B
GR-1-C	hibonite core	0.2 ±0.1	1515	94‡	0.14 ±0.05	5.99%	1336	4240‡	10‡	1.3‡ ±0.3	<0.03	0.02%	85	481§ 346-937	131§ 19-307	GR-1-C
GR-1-R	hibonite rim	40	2750	384‡	46	5.99%	449	4510‡	38‡	2.9‡	0.7‡ ±0.2	0.02%	10	20	11	GR-1-R
GR-1-M	corundum	53	23	2155	54	663	150	1695	9.3 ±1.0	12.8 ±1.3	1.6 ±0.3	0.02%	2.6 ±0.4	0.9 ±0.2	3.4 ±1.0	GR-1-M
GR-1-B◊	hib. + cor. bulk	158	881	7455	220	1.22%	495	1799	13	175	23	—	15	135	118	GR-1-B
HAL	hibonite	7	231	57	0.7	5.98%	236	3812	0.4 ±0.1	0.3 ±0.1	29	0.49%	70	4.0 ±0.2	23	HAL
DH-H1	hibonite	13	62	314	5.9	5.99%	113	541	<0.12	30	4.5 ±0.7	0.34%	74	3.6 ±0.5	11.2 ±1.4	DH-H1
C1 Chondrites		4916	9.529%	10.57%	544.2	8998	6.066	426.2	55.65	2606	1887	18.32%	7.715	1.520	3.182	C1's

*Determined by electron microprobe (MUCH-1, BB-5 by MACPHERSON *et al.*, 1983; GR-1 by MACPHERSON *et al.*, 1984; HAL by ALLEN *et al.*, 1980; DH-H1 by HINTON and BISCHOFF, 1984). †Determined in an analysis of a separate spot. ‡These elements may be high due to overlap onto corundum. §Variable Y and Zr due to overlap onto zirconium oxide grains. ◊Rastered beam analysis.

the large hibonite grain by an unknown sodium-rich phase (possibly glass) and nepheline. These sodium-rich phases differ in chemical composition from fine-grained alkali-rich material present within the surrounding matrix.

3. EXPERIMENTAL

All analyses reported in this work were obtained with a modified AEI IM-20 ion microprobe at the University of Chicago. Polished thin sections were bombarded with a primary beam of 20 keV $^{16}O^-$ ions focussed into a 5–20 μm spot. The primary beam current was 1–5 nA for isotopic measurements and up to 15 nA for trace element analyses. Details of analytical methods for measurement of calcium and magnesium isotopic compositions and concentrations of REE and other trace elements are given in the Appendix. The analytical method for titanium isotopic measurement of HAL hibonite was reported by HINTON *et al.* (1987b).

4. COMPARISON WITH PREVIOUS ANALYSES

Minor and trace element analyses of hibonite and other phases are given in Table 1. Iron is the only element which occurs in concentrations of 1000 ppm or more that was not determined by ion microprobe, so electron microprobe values are included in Table 1, where available. Barium and lanthanide analyses of the same samples are given in Table 2. The C1 chondrite normalization values in these tables were calculated by A. M. DAVIS (in prep.), using methods similar to those used by ANDERS and EBIHARA (1982) with some additional recent analytical data. C1 chondrite-normalized REE patterns are shown in Figs. 1–4. Comparisons with literature values for lanthanides are shown in the Figs. 1, 2 and 4. A comparison between ion microprobe and literature values for elements not shown in the figures is given in Table 3. Magnesium and calcium isotopic results on hibonite are given in Table 4. Errors were calculated assuming that all uncertainty was due to counting statistics. All errors given in the tables and figures are $\pm 2\sigma$.

4.1 DJ-1

The calcium and titanium concentrations determined by electron and ion microprobe are in good agreement, but the electron microprobe value for magnesium is significantly higher than the ion microprobe value (Table 3). The electron microprobe analysis was done using an energy-dispersive detector. In this method of analysis, magnesium and silicon are often difficult to determine accurately, because the small magnesium and silicon K_α peaks cannot be completely resolved from the large aluminum K_α peak. For this reason, the EDS magnesium and silicon analyses are believed to be inaccurate.

4.2 MUCH-1

The ion microprobe data reported in Table 2 are higher than the INAA data of EKAMBARAM *et al.* (1984, 1985) for all REE except lutetium. There is some uncertainty in the absolute concentrations determined by INAA because the microbalance used to weigh the sample was faulty. Therefore, we have normalized the INAA analyses to the Ca concentration in Table 1. After this normalization LREE have the same enrichments for both techniques (Fig. 1), but the INAA levels of terbium, dysprosium, holmium and thulium are a factor ~1.3 lower, europium a factor of ~1.7 higher and lutetium a factor of ~2.7 higher than the ion microprobe values (Fig. 1b). This discrepancy can be explained if MUCH-1 hibonite is zoned, as has been observed in unpublished REE data on hibonite from Murchison inclusion SH-7 (described in HASHIMOTO *et al.*, 1986) and Allende inclusion 3529-42 (described in MACPHERSON *et al.*, 1986). Sodium, chromium and manganese contents given by INAA (EKAMBARAM

Table 2. Barium and lanthanide concentrations, in ppm. All uncertainties are ±2σ based on counting statistics.

Sample	Phase	Ba	La	Ce	Pr	Nd	Sm	Eu	Gd	Tb	Dy	Ho	Er	Tm	Yb	Lu	Sample
DJ-1	hibonite	13.92 ±0.29	11.79 ±0.22	29.01 ±0.41	4.89 ±0.15	23.85 ±0.40	7.70 ±0.26	0.67 ±0.04	9.71 ±0.65	1.39 ±0.12	8.49 ±0.36	1.39 ±0.09	2.54 ±0.19	0.20 ±0.03	<0.24	0.13 ±0.05	DJ-1
MUCH-1	hibonite	10.41 ±0.41	13.62 ±0.40	34.57 ±0.73	5.36 ±0.26	26.44 ±0.69	8.13 ±0.44	0.56 ±0.06	12.79 ±1.29	2.32 ±0.26	14.56 ±0.76	2.96 ±0.22	7.25 ±0.47	0.75 ±0.10	0.34 ±0.25	0.20 ±0.09	MUCH-1
BB-6	hibonite	68.2 ±1.9	8.0 ±0.6	26.4 ±1.2	3.5 ±0.4	17.4 ±1.0	5.6 ±0.7	0.90 ±0.16	2.6 ±1.1	0.53 ±0.24	1.6 ±0.6	0.39 ±0.15	0.46 ±0.31	0.42 ±0.14	0.76 ±0.30	<0.12	BB-6
BB-5-1	hibonite	13.78 ±0.49	11.53 ±0.38	27.54 ±0.67	4.48 ±0.24	21.05 ±0.64	6.44 ±0.41	0.69 ±0.07	8.67 ±1.02	1.46 ±0.21	7.68 ±0.57	1.39 ±0.15	2.92 ±0.33	0.31 ±0.07	0.49 ±0.23	0.26 ±0.08	BB-5-1
BB-5-2	hibonite + perov.	7.17 ±0.74	5.23 ±0.54	13.4 ±1.0	2.48 ±0.37	11.7 ±1.0	4.88 ±0.74	0.70 ±0.17	8.9 ±2.8	2.16 ±0.55	14.9 ±2.7	2.66 ±0.49	4.29 ±0.92	0.39 ±0.16	0.61 ±0.60	0.30 ±0.21	BB-5-2
BB-5-C*	corundum	≤0.01			Σ(La - Eu) ≤ 0.01				≤0.04	≤0.02	≤0.08	≤0.02	≤0.05	≤0.01	≤0.01	≤0.01	BB-5-C
BB-5-O*	corundum + 2 unk.	3.06 ±0.19	0.63 ±0.07	0.61 ±0.08	0.40 ±0.06	3.43 ±0.21	1.91 ±0.19	0.32 ±0.04	18.4 ±1.3	2.38 ±0.24	18.7 ±1.0	4.6 ±0.2	15.9 ±0.6	2.75 ±0.16	1.76 ±0.32	3.82 ±0.20	BB-5-O
BB-5-A*	corundum + unk. #1	≤0.1	≤0.6	≤0.3	≤0.4	≤0.5	≤0.5	≤0.6	3.1 ±1.4	0.8 ±0.5	8.7 ±1.8	3.8 ±1.2	15.1 ±2.9	2.9 ±1.0	<0.5	3.7 ±1.2	BB-5-A
BB-5-B*	corundum + unk. #2	5.3 ±1.2	≤0.5	≤0.9	≤0.4	2.8 ±1.0	1.6 ±1.0	≤0.3	21.4 ±2.4	2.7 ±0.8	14.3 ±1.8	3.5 ±0.9	5.7 ±1.2	0.81 ±0.43	—	<1.2	BB-5-B
GR-1-C	hibonite core	19.6 ±0.6	90.7 ±1.2	108.7 ±1.5	27.1 ±0.6	207.0 ±2.1	38.0 ±1.1	1.36 ±0.12	316.1 ±5.7	46.9 ±1.2	256.4 ±2.9	42.1 ±0.8	73.7 ±1.7	3.37 ±0.23	<2.2	5.12 ±0.48	GR-1-C
GR-1-R*	hibonite rim	0.92 ±0.19	0.36 ±0.09	0.56 ±0.14	0.20 ±0.07	0.44 ±0.14	0.33 ±0.14	0.13 ±0.05	0.5 ±0.5	0.33 ±0.14	2.43 ±0.47	0.78 ±0.15	1.54 ±0.29	0.17 ±0.07	0.17 ±0.15	0.09 ±0.07	GR-1-R
GR-1-M*	corundum	0.04 ±0.01	0.08 ±0.01	0.13 ±0.02	0.01 ±0.01	0.07 ±0.01	0.02 ±0.01	0.002 ±0.001	0.04 ±0.03	0.02 ±0.01	0.11 ±0.03	0.03 ±0.01	0.10 ±0.02	0.01 ±0.01	0.02 ±0.01	0.02 ±0.01	GR-1-M
GR-1-B*†	hib. + cor. bulk	5.46 ±0.37	—	—	—	—	—	—	35.3 ±2.2	5.26 ±0.43	27.8 ±1.2	5.00 ±0.33	8.48 ±0.64	0.46 ±0.10	0.41 ±0.35	0.70 ±0.17	GR-1-B
HAL	hibonite	7.49 ±0.16	13.10 ±0.18	0.062 ±0.014	3.28 ±0.09	16.89 ±0.25	3.49 ±0.13	0.99 ±0.04	2.80 ±0.28	0.28 ±0.05	1.47 ±0.13	0.26 ±0.03	0.36 ±0.07	0.06 ±0.02	0.12 ±0.08	0.07 ±0.02	HAL
DH-H1	hibonite	0.48 ±0.06	25.54 ±0.38	0.037 ±0.016	1.44 ±0.09	30.21 ±0.52	5.68 ±0.26	1.12 ±0.07	4.27 ±0.52	0.46 ±0.10	1.97 ±0.24	0.29 ±0.05	0.38 ±0.12	0.05 ±0.03	0.19 ±0.12	0.12 ±0.04	DH-H1
C1 Chondrites		2.299	0.2347	0.6032	0.08908	0.4524	0.1471	0.05600	0.1966	0.03633	0.2427	0.05556	0.1589	0.02416	0.1625	0.02431	C1's

*Absolute lanthanide abundances based on the Y content and the mean Ho/Y in C1 chondrites. †Rastered beam analysis; no LREE values given because of overlap onto adjacent Madagascar hibonite standard.

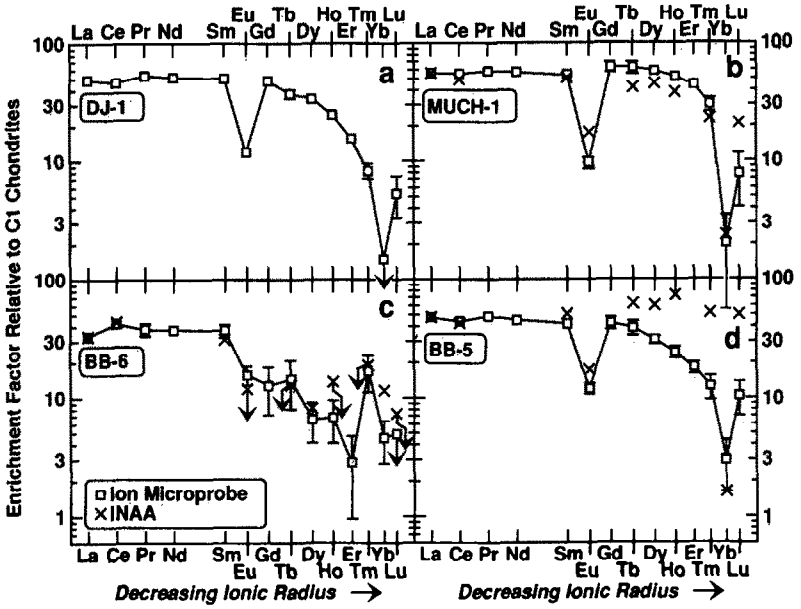

FIG. 1. Enrichment factors relative to C1 chondrites for REE in Murchison hibonite. Uncertainties shown are $\pm 2\sigma$, based on counting statistics. Enrichment factors for bulk inclusions BB-5 and MUCH-1 (EKAMBARAM *et al.*, 1984, 1985) are normalized to the calcium concentration determined in this work.

et al., 1984) are substantially higher than those given by ion microprobe (Table 3), suggesting that the hibonite sample hand picked for INAA had a minor amount of iron-rich phyllosilicate adhering to it. The INAA strontium concentration is substantially higher than the ion microprobe value, but has a large uncertainty (302 ± 224 ppm Sr, calcium-normalized, $\pm 2\sigma$).

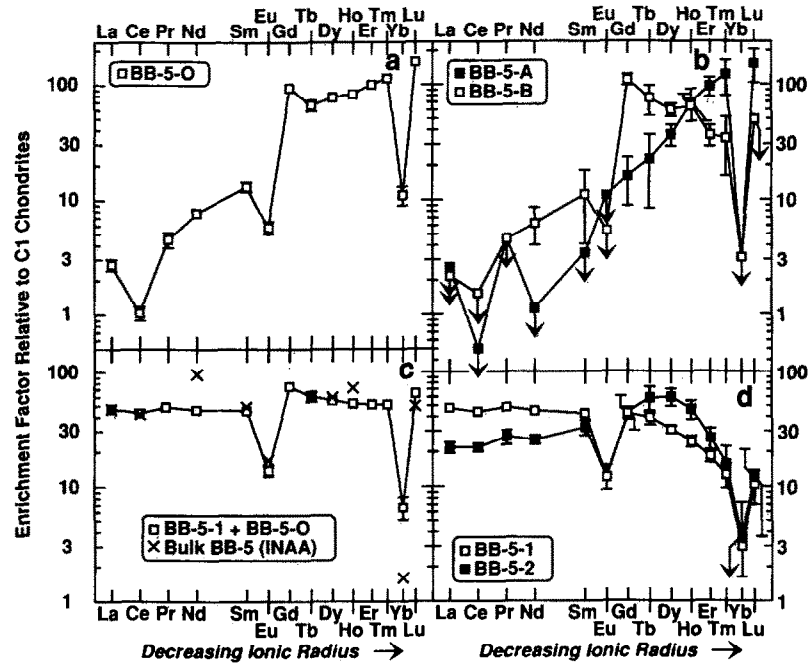

FIG. 2. Enrichment factors relative to C1 chondrites for REE in selected areas of BB-5. Uncertainties shown are $\pm 2\sigma$, based on counting statistics. (a) BB-5-O consists of combined runs on two HREE-rich phases within corundum. The individual analyses most closely approaching compositions of the two pure phases in BB-5-O are shown in (b): BB-5-A is a low Gd/Lu, HREE-rich phase within corundum, believed to be zirconium oxide; BB-5-B is a high Gd/Lu, HREE-rich phase within corundum, believed to be hibonite. Enrichment factors in BB-5-A and BB-5-B are minimum values because of uncorrected overlap onto REE-free corundum. (c) Mixing of 27% BB-5-O and 73% BB-5-1 matches the REE pattern of bulk BB-5 (EKAMBARAM *et al.*, 1984, 1985) quite well except for ytterbium. The uncertainty in neodymium in the bulk pattern (not shown) overlaps neodymium in the calculated pattern. (d) BB-5-1 is pure hibonite and BB-5-2 is hibonite containing a small amount of perovskite.

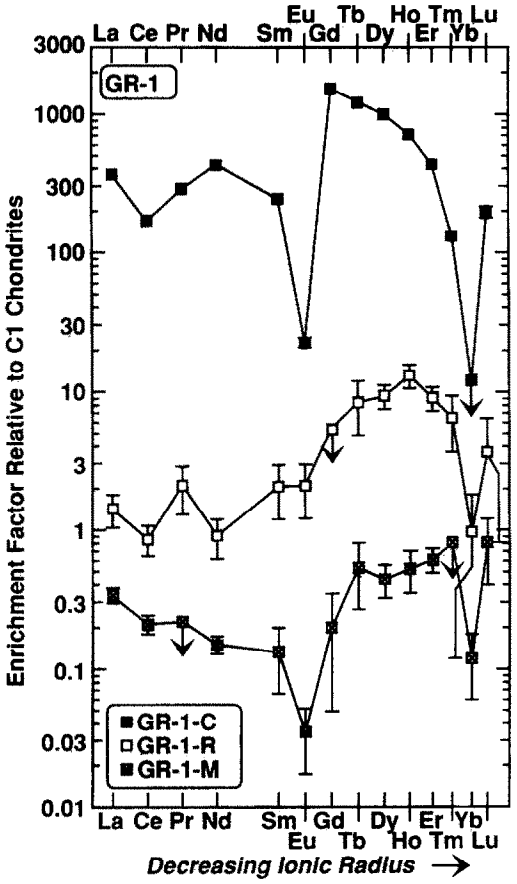

FIG. 3. Enrichment factors relative to C1 chondrites for REE in hibonite and corundum from the Murchison inclusion GR-1. Uncertainties shown are $\pm 2\sigma$, based on counting statistics. GR-1-C and GR-1-R are core and rim hibonite, respectively. GR-1-M is mantle corundum, which separates GR-1-C from GR-1-R.

4.3 BB-6

Previously unpublished electron microprobe analyses of BB-6 hibonite by G. J. MacPherson are given in Table 3. The hibonite analyzed by ion microprobe is lower in magnesium and higher in silicon than that analyzed by electron microprobe. The electron microprobe analyses may be incorrect, since they were done using an energy-dispersive detector. Sample heterogeneity is also possible. The observed Ca/La ratio measured by ion microprobe is over an order of magnitude higher than INAA upper limit given by EKAMBARAM *et al.* (1984), but reexamination of the INAA data revealed an error in calculation of the CaO concentration of BB-6. The correct INAA 2σ upper limit is <6.9 wt% CaO or <4.9 wt% Ca. INAA and ion microprobe REE patterns agree well for all elements analyzed except ytterbium (Fig. 1c), for which the INAA value is higher by a factor of ~2.5. There may be another REE-bearing phase with a different REE pattern in the INAA sample. Perovskite, observed by MACPHERSON *et al.* (1983), may be that second phase. The INAA chromium content is 6 times higher than the ion microprobe value, perhaps because some matrix adhered to the INAA sample. The scandium concentration measured by ion microprobe is 2.5 times higher than the INAA value. The reason for this is not known.

4.4 BB-5

Major and minor element compositions of corundum (BB-5-C) and hibonite (BB-5-1) determined by ion microprobe are compared with electron microprobe values of BAR-MATTHEWS *et al.* (1982) in Table 3. There are significant discrepancies for silicon and calcium in corundum and vanadium in hibonite, where electron microprobe values are two, one-half and four times ion microprobe values, respectively. A possible explanation for these differences is that these electron microprobe values are near detection limits.

Although calcium and lanthanum contents determined by INAA in bulk BB-5 (EKAMBARAM *et al.*, 1984) are lower than the ion microprobe contents of these elements in BB-5-1 hibonite (Tables 1 and 2) by ~30%, the Ca/La ratios measured by the two techniques agree. The ion microprobe analysis demonstrates that corundum, an abundant phase in BB-5, is extremely low in all trace elements except titanium and scandium. In order to compare ion microprobe data on hibonite with INAA data on bulk BB-5, dilution by trace element-poor corundum was corrected for by normalizing the INAA data to

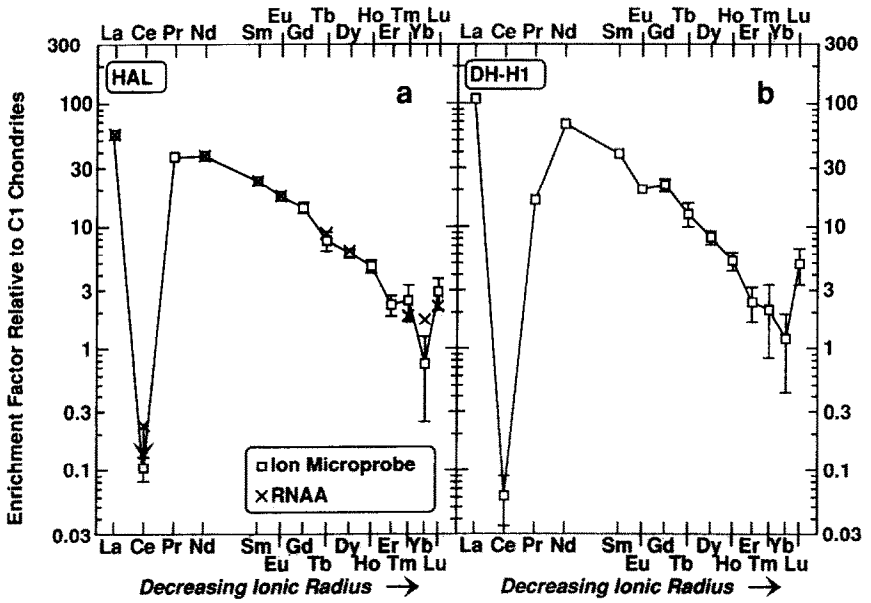

FIG. 4. Enrichment factors relative to C1 chondrites for REE in Allende inclusion HAL and Dhajala inclusion DH-H1. Uncertainties shown are $\pm 2\sigma$, based on counting statistics.

Table 3. Comparison of ion microprobe (IP) analyses with literature analyses by instrumental neutron activation analysis (INAA) and electron microprobe analysis using energy-dispersive (EDS) or wavelength-dispersive (WDS) spectrometers. All results are given in ppm unless otherwise indicated. INAA analyses of MUCH-1 and BB-5 hibonite were normalized to the Ca concentration given in Table 1. MUCH-1 was used as a Sc standard.

Sample	Method	Na	Mg	Si	Ca	Sc	Ti	V	Cr	Mn	Sr	Y	Zr	Sample
DJ-1	IP	4	3075	83	5.98%	535	7517	24	0.8	0.6	64	41	90	DJ-1
hibonite	EDS[1]	—	0.60%	—	6.21%	—	0.89%	—	—	—	—	—	—	hibonite
MUCH-1	IP	27	4643	1889	5.97%	≅455	1.01%	34	7.9	15	68	76	122	MUCH-1
hibonite	EDS[2]	—	0.65%	—	6.22%	—	1.23%	—	—	—	—	—	—	hibonite
	INAA[3]	250	<14%	—	5.97%	455	<3.3%	<0.079%	468	76	302	—	<245	
BB-6	IP	73	1.35%	4127	5.93%	33.3	2.71%	247	192	132	136	≤4.0	51	BB-6
hibonite	EDS[1]	—	2.39%	0.22%	5.68%	—	3.38%	—	—	—	—	—	—	hibonite
	INAA[3]	<74	—	—	<4.9%	13.1	—	<0.52%	1108	<50	<250	—	<220	
BB-5-1	IP	3.1	4170	56	5.96%	483	9052	53	2.0	0.5	75	39	102	BB-5-1
hibonite	WDS[4]	—	0.39%	0.005%	5.96%	—	1.21%	0.02%	—	—	—	—	—	hibonite
	INAA[3]	259	<6.0%	—	5.96%	497	<1.5%	<0.023%	36	54	<162	—	223	
BB-5-C	IP	0.3	7.3	93	125	289	2534	17	0.6	<0.1	0.5	0.6	3.1	BB-5-C
corundum	WDS[4]	—	<0.012%	0.019%	70	—	0.19%	—	—	—	—	—	—	corundum
GR-1-C	IP	0.2	1515	94	5.99%	1316	4176	10	1.3	0.01	84	474	129	GR-1-C
hibonite	WDS[5]	—	0.15%	<0.019%	5.88%	0.10%	0.38%	<0.014%	<0.03%	—	—	—	—	hibonite
GR-1-R	IP	39	2750	384	5.99%	442	4442	37	2.9	0.7	10	20	11	GR-1-R
hibonite	WDS[5]	—	0.23%	<0.019%	5.92%	0.05%	0.61%	<0.014%	<0.03%	—	—	—	—	hibonite
GR-1-M	IP	53	23	2155	663	150	1695	9.3	12.8	1.6	2.6	0.9	3.4	GR-1-M
corundum	WDS[5]	—	<0.012%	<0.019%	0.01%	0.05%	0.11%	<0.014%	<0.03%	—	—	—	—	corundum
HAL	IP	7	231	57	5.98%	236	3812	0.4	0.3	29	70	4.0	23	HAL
hibonite	WDS[6]	—	<0.006%	<0.009%	6.22%	0.03%	0.43%	<0.014%	<0.014%	—	—	<0.02%	<0.02%	hibonite
	INAA[7]	297	<3.6%	<1.2%	5.36%	452	0.50%	<57	<3.6	20.9	<285	—	<65	
DH-H1	IP	13	62	314	5.99%	113	541	0.03	30	4.7	74	3.6	11.2	DH-H1
hibonite	WDS[8]	<74	<0.012%	0.12%	6.36%	—	<0.03%	—	<0.05%	—	—	—	—	hibonite

1. Unpublished analysis by G. J. MacPherson. 2. MACPHERSON *et al.* (1983). 3. EKAMBARAM *et al.* (1984, 1985). 4. BAR-MATTHEWS *et al.* (1982). 5. MACPHERSON *et al.* (1984). 6. ALLEN *et al.* (1980). 7. DAVIS *et al.* (1982). 8. HINTON and BISCHOFF (1984).

the Ca concentration in Table 1. The calcium-normalized INAA concentration of Zr is 2.2 times higher than the ion microprobe value (Table 3). Although the INAA value has a large uncertainty, the higher zirconium in bulk may be due to tiny zirconium-rich oxide grains found in corundum by ion microprobe (see section 5.5). Volatile element concentrations measured by ion microprobe in BB-5-1 are significantly lower than the normalized INAA values (Table 3). A minor amount of the phyllosilicate observed by BAR-MATTHEWS *et al.* (1982) may have adhered to the INAA sample.

Comparison of the REE pattern in BB-5-1 hibonite with that of calcium-normalized bulk BB-5 shows that both have similar LREE enrichments but the bulk is higher in HREE than BB-5-1 (Fig. 1d). The HREE in BB-5 are carried by perovskite and at least two other refractory oxide phases (Fig. 2), described in detail in section 5.5.

4.5 GR-1

Analyses of minor elements in corundum and core and rim hibonite from GR-1 are in reasonable agreement with those of MACPHERSON *et al.* (1984), Table 3, except for calcium and titanium in corundum, for which ion microprobe values are significantly higher. A small amount of perovskite may have been included in the ion microprobe analysis area.

4.6 HAL

Most major and trace element concentrations measured for hibonite in this work are in good agreement with those measured by INAA, radiochemical neutron activation analysis (RNAA) (DAVIS *et al.*, 1982) and electron microprobe (ALLEN *et al.*, 1980) (Table 3; Fig. 4). The minor differences are probably related to chemical zoning observed within HAL hibonite (ALLEN *et al.*, 1980; DAVIS *et al.*, 1982). The Sc concentration determined by ion microprobe is significantly lower than the two INAA values, but within the range of values determined by electron microprobe (ALLEN *et al.*, 1980). The high sodium content measured by INAA is probably due to the presence of alkali-rich phases on surfaces of hibonite (ALLEN *et al.*, 1980). The Yb concentration determined by ion microprobe in HAL hibonite is lower than the two RNAA values by factors of 2.6 ± 1.7 and 2.0 ± 1.4 (±2σ). The reason for this discrepancy is not known.

The Δ^{44}Ca value obtained for HAL hibonite, +7.0 ± .9‰/amu, is in very good agreement with that obtained by LEE *et al.* (1979) using thermal ionization mass spectrometry, +6.8 ± .1‰/amu and that obtained by FAHEY *et al.* (1987a) by ion microprobe, +7.7 ± 1.8‰/amu. Magnesium in HAL hibonite is of normal isotopic composition, also in agreement with the data of LEE *et al.* (1979). Only ^{47}Ti and ^{49}Ti could be measured in HAL hibonite, because of the presence of interferences from $^{30}Si^{16}O$ at mass 46, ^{48}Ca at mass 48 and $^{23}Na^{27}Al$ at mass 50. The $^{47}Ti/^{49}Ti$ ratio of HAL hibonite is lower than that of normal titanium. Since FAHEY *et al.* (1987a) found no nuclear isotopic anomalies at these masses in HAL hibonite, we conclude that titanium in HAL hibonite is enriched in the heavy isotopes by 5 ± 1‰/amu. FAHEY *et al.* (1987a) measured all masses of titanium in HAL hibonite and found a titanium mass fractionation of +4.4 ± 2.2‰/amu, based on ^{46}Ti, ^{47}Ti and ^{49}Ti.

4.7 DH-H1

The Si concentration given by electron microprobe is substantially higher than that found by ion microprobe (Table 3). There may have been fluorescence from surrounding silica-rich matrix during electron microprobe analysis. The Ti concentration found by ion microprobe is somewhat higher than the limit set by electron microprobe. Ion microprobe analyses of several spots within DH-H1 hibonite showed that titanium concentrations are uniform. The reason for this discrepancy is not known.

5. RESULTS AND DISCUSSION

5.1 Trace element patterns in hibonite

The trace element patterns of hibonite have a number of features in common. In Fig. 5, C1 chondrite-normalized enrichment factors for trace elements (including selected REE) in the mean of DJ-1 and MUCH-1 hibonite are plotted in order of volatility. These enrichment factors range over five orders of magnitude. All hibonite shows an enrichment in refractory relative to volatile trace elements, but this enrichment is not entirely due to volatility. In solar nebula condensation or evaporation models in which hibonite is permitted to equilibrate with the surrounding gas and with coexisting trace element-bearing phases, the concentration of each trace element in hibonite depends on a number of factors: temperature, pressure, the amount of trace element in the system (hibonite plus its environment), the volatility of that trace element, the ease with which the trace element can substitute into the hibonite lattice and the quantities present of other trace element-bearing phases with which hibonite has partitioned. In order to compensate for the effect of solubility in hibonite and to facilitate comparison of different hibonite samples with one another, the trace element concentrations in all hibonite have been normalized to the mean of concentrations in DJ-1 and MUCH-1 in Fig. 6. DJ-1 and MUCH-1 were chosen because they appear to have come from group III refractory inclusions (see discussion of individual hibonite samples). In group III inclusions, all refractory lithophiles are enriched to the same degree, with the exception of europium, ytterbium, strontium and barium, which are somewhat depleted (MARTIN and MASON, 1974; MASON and MARTIN, 1977). Ideally, hibonite chosen for normalization should come from an internally equilibrated inclusion with uniform enrichments of all refractory elements, such as a once-molten group I inclusion. Unfortunately, the suite of trace elements reported here have not yet been determined in hibonite from such an inclusion. In the two hibonite samples chosen for normalization, the Eu/Eu* and Yb/Yb* ratios range from 0.11 ± .08 to .24 ± .02 (±2σ). [A europium or ytterbium anomaly (Eu/Eu* or Yb/Yb*) is defined as the measured enrichment factor relative to C1 chondrites divided by that calculated by averaging the enrichment factors of adjacent REE.] This degree of fractionation is relatively minor compared to five orders of magnitude of variation in enrichments plotted in Fig. 6 and the eight orders of magnitude variation in trace element enrichment factors in all of the hibonite analyzed in this work. The remaining inclusions were not used for normalization because (1) sodium and magnesium in BB-5-1 were determined in a separate analysis from other minor and trace elements, (2) BB-6 and GR-1 seem to have experienced significant gas-solid fractionation

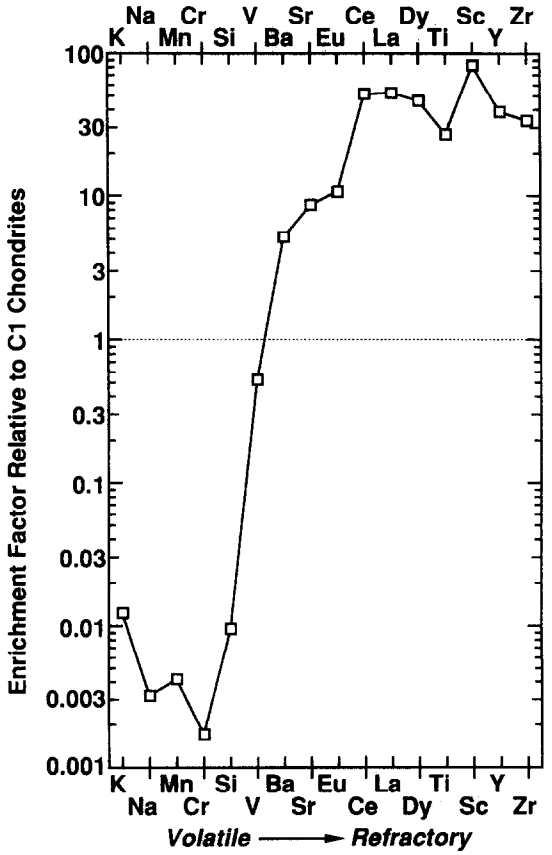

FIG. 5. C1 chondrite-normalized enrichment factors of trace elements in the mean of DJ-1 and MUCH-1 hibonite, in order of increasing refractoriness.

Table 4. Nuclear isotopic anomalies in magnesium and isotopic mass fractionation of magnesium, calcium and titanium. Uncertainties are ±2σ. Only in DH-H1 does δ^{26}Mg vary with Al/Mg.

Sample	Δ^{25}Mg* (‰/amu)	δ^{26}Mg† (‰)	Δ^{44}Ca‡ (‰/amu)	Δ^{46}Ti§ (‰/amu)
DJ-1	-2.2 ± 2.6	+1.9 ± 3.3	-0.5 ± 1.5	+4.0 ± 1.6
BB-5	-7.0 ± 3.2	+5.8 ± 2.4	-3.7 ± 0.6	+1.3 ± 1.0
GR-1(core)	-4.4 ± 1.8	-0.8 ± 3.3	-2.6 ± 1.9	+1.1 ± 1.9
GR-1(rim)	-6.5 ± 2.7	-1.7 ± 1.8	-7.3 ± 1.4	+0.4 ± 2.9
HAL	-2 ± 5◊	+1.2 ± 3.8◊	+7.0 ± 0.9	+5.5 ± 0.9
DH-H1	+18.9 ± 5.7◊	+66 to +920◊	+12.5 ± 1.2	—

*$\Delta^{25}Mg = \dfrac{(^{25}Mg/^{24}Mg)_{unknown} - (^{25}Mg/^{24}Mg)_{standard}}{(^{25}Mg/^{24}Mg)_{standard}} \times 1000.$

†$\delta^{26}Mg = \dfrac{(^{26}Mg/^{24}Mg)_{unknown} - (^{26}Mg/^{24}Mg)_{standard}}{(^{26}Mg/^{24}Mg)_{standard}} \times 1000,$

corrected for mass fractionation using Δ^{25}Mg.

‡$\Delta^{44}Ca = \dfrac{(^{44}Ca/^{40}Ca)_{unknown} - (^{44}Ca/^{40}Ca)_{standard}}{(^{44}Ca/^{40}Ca)_{standard}} \times \dfrac{1000}{4}.$

§$\Delta^{46}Ti = -\dfrac{(^{46}Ti/^{48}Ti)_{unknown} - (^{46}Ti/^{48}Ti)_{standard}}{(^{46}Ti/^{48}Ti)_{standard}} \times \dfrac{1000}{2}$, data of HINTON *et al.* (1987b).

◊data of HINTON and BISCHOFF (1984).

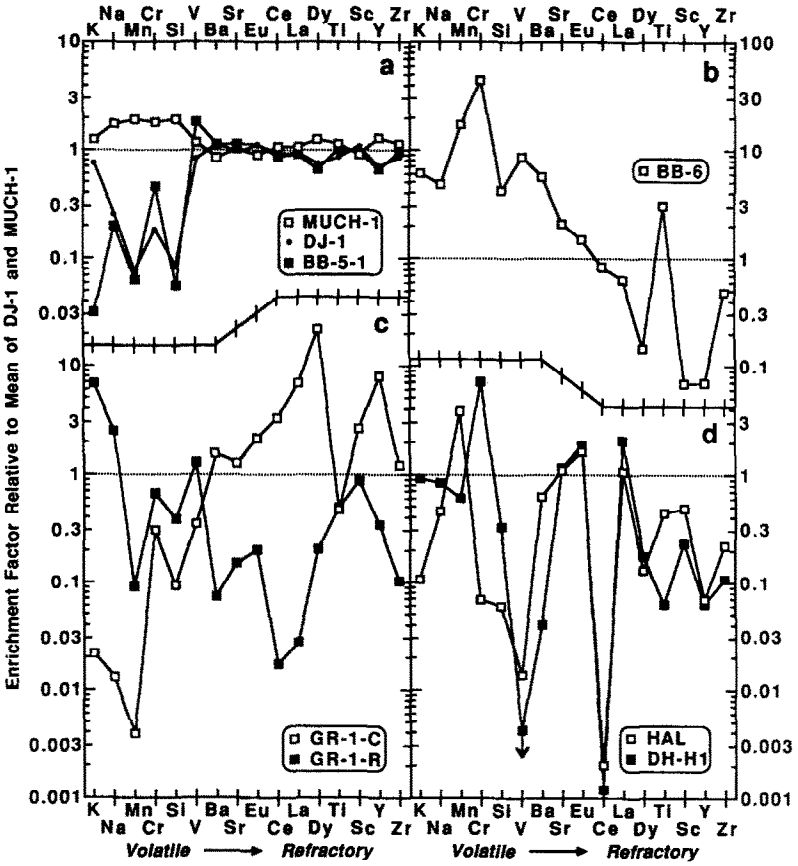

FIG. 6. Trace element abundances in hibonite, normalized to the mean of concentrations in DJ-1 and MUCH-1 hibonite. The elements are plotted in order of volatility. (a) DJ-1, MUCH-1 and BB-5-1 have very similar refractory element patterns and somewhat variable volatile element patterns. (b) BB-6 is richer in volatile and poorer in refractory trace elements than the other hibonite analyzed in this work. (c) GR-1-C is higher in refractory and lower in volatile elements than GR-1-R. (d) HAL and DH-H1 are strongly depleted in vanadium and cerium, indicating high temperature formation in an oxidizing environment.

at such high temperatures that LREE are fractionationed from HREE by volatility, and (3) HAL and DH-H1 seem to have come from a highly oxidizing environment (see sections 5.4, 5.6 and 5.7).

5.2 DJ-1

The C1 chondrite-normalized enrichment factors of REE in DJ-1 are quite uniform for LREE and drop smoothly through HREE (Fig. 1a). Superimposed are negative europium and ytterbium anomalies, $Eu/Eu^* = 0.236 \pm .029$ and $Yb/Yb^* = 0.063 \pm .156$ ($\pm 2\sigma$). Within analytical uncertainty, these anomalies can be of the same magnitude. Smooth REE patterns with negative europium and ytterbium anomalies of similar magnitude were first recognized in Allende refractory inclusions by MARTIN and MASON (1974). In these group III inclusions all REE except europium and ytterbium have the same C1 chondrite-normalized enrichment factor. These patterns are thought to arise because europium and ytterbium, the least refractory REE in a gas of solar composition (BOYNTON, 1975; DAVIS and GROSSMAN, 1979), had failed to condense when the inclusions were removed from a cooling solar nebular gas. These elements would also be the first REE lost if the inclusions formed by volatilization.

Hibonite appears to favor LREE over HREE in partitioning with the other phases likely to be found in refractory inclusions. A number of REE partitioning studies have been done on hibonite, perovskite, melilite and fassaite, phases that are the major carriers of REE in refractory inclusions. Partitioning of REE between hibonite and a silicate liquid in the $CaTs_{90}Di_{10}$ system gives a hibonite/liquid partition coefficient for lanthanum that is 69 ± 24 ($\pm 1\sigma$) times that of ytterbium, (DRAKE and BOYNTON, 1988). In a system containing 32 wt% TiO_2, 30 wt% SiO_2 and 38 wt% CaO, perovskite/liquid partition coefficients drop by a factor of 6 from lanthanum to lutetium (NAGASAWA *et al.*, 1980). Similar experiments done with melilite in a system containing 41 wt% CaO, 5 wt% MgO, 26 wt% Al_2O_3 and 28% wt% SiO_2 show a drop in partition coefficient by a factor 2 from lanthanum to lutetium (NAGASAWA *et al.*, 1980). A number of studies show that diopside favors HREE relative to LREE compared to silicate liquids (IRVING, 1978). The structure of silicate melts can affect REE partition coefficients (MYSEN and VIRGO, 1980), but the REE patterns of coexisting phases in refractory inclusions are generally in agreement with the partitioning experiments. HINTON and DAVIS (1986a) showed that fassaite and melilite in a once-molten Allende refractory inclusion have higher and lower HREE/LREE ratios than the bulk,

respectively, in agreement with separate melilite-liquid and pyroxene-liquid partitioning experiments. HASHIMOTO *et al.* (1986) measured REE in adjacent hibonite and perovskite in Murchison inclusion SH-7. Assuming that these phases are in equilibrium, hibonite/perovskite partition coefficients decrease by a factor of ~120 from lanthanum to lutetium. Although the silicate liquids in the partitioning experiments differ in composition and probably differ in partitioning behavior, there can be little doubt that hibonite has the strongest preference for LREE over HREE of the REE-bearing minerals commonly found in refractory inclusions.

If REE were partitioned among the phases of a group III inclusion, hibonite separated from that inclusion should have an enrichment of LREE over HREE, no matter which of the other common REE-bearing phases were present during partitioning. This partitioning can take place during crystallization from a melt or during cocondensation of several REE-bearing phases. The degree of enrichment of LREE over HREE in hibonite depends on the identities and amounts of other phases involved in partitioning. If the condensed phases in the system in which partitioning took place were depleted in europium and ytterbium due to volatility, then ytterbium and europium depletions would be expected to be superimposed on the otherwise smoothly fractionated REE pattern of hibonite. This is what is qualitatively observed in DJ-1 (Fig. 1). The minerals with which DJ-1 hibonite partitioned REE are now missing. Perhaps an original DJ-1 inclusion was friable because it was a fluffy aggregate of condensate grains or because other primary minerals were replaced during alteration. It is unclear whether the loss of the other primary or secondary minerals took place prior to parent body formation or in the freeze-thaw disaggregation and density separation. It is also possible that the minerals that condensed with DJ-1 hibonite never accreted with it.

5.3 *MUCH-1*

MUCH-1 hibonite has negative europium and ytterbium anomalies of similar magnitude: $Eu/Eu^* = 0.166 \pm .020$ and $Yb/Yb^* = 0.107 \pm .082$ (Fig. 1b). Apart from europium and ytterbium, the LREE pattern of MUCH-1 is flat and HREE drop smoothly in C1 chondrite-normalized enrichment factor from gadolinium to lutetium. There appears to be a step up in enrichment factor between LREE and HREE. The INAA analysis of MUCH-1 gives a similar REE pattern, but shows a step downwards from LREE to HREE (Fig. 1b). Similar small steps, both up and down, have been observed in REE patterns from the Murchison hibonite-rich inclusion SH-7 (HASHIMOTO *et al.*, 1986; unpublished work from this laboratory), so the differences between the ion microprobe and INAA REE patterns for MUCH-1 may be due to sample heterogeneity. If the REE content of MUCH-1 hibonite were controlled by igneous partitioning in a reservoir with C1 chondritic proportions of REE, lanthanide enrichment factors in it should be a smooth function of atomic number. Gas/solid fractionation in a reservoir with C1 chondritic proportions of REE can lead to irregular REE patterns, because REE volatilities are not a smooth function of atomic number and the LREE as a group are significantly less refractory than all HREE except ytterbium (BOYNTON, 1975; DAVIS and GROSSMAN, 1979). Hibonite with a smoothly fractionated, but stepped REE pattern could also be produced by igneous partitioning in a reservoir with a stepped bulk REE pattern. Preservation of hibonite with steps going both up and down, however, could not be caused by igneous partitioning, regardless of bulk composition. The most likely explanation is that these stepped patterns preserve the condensation history of hibonite, in which hibonite grains passed through gases of changing composition as they grew. A hibonite grain having a REE pattern with a step up from LREE to HREE could be formed by removing the grain from equilibrium with the gas at a temperature such that the LREE have not completely condensed. If another grain of hibonite with REE fully condensed (*i.e.*, having a smooth REE pattern) then came into equilibrium with this gas at lower temperature, only LREE would be added and this hibonite would end up with a REE pattern with a step down from LREE to HREE.

DJ-1 and MUCH-1 have similar concentrations of refractory elements, but MUCH-1 is significantly higher in sodium, manganese, chromium and silicon than DJ-1 (Fig. 6). MUCH-1 hibonite is surrounded by a highly altered region of calcite and gypsum with minor perovskite (MACPHERSON *et al.*, 1983). Some volatile elements may have been introduced into hibonite during alteration.

REE patterns in MUCH-1 hibonite determined by INAA and ion microprobe can only be explained by condensation of hibonite with at least one other REE-bearing phase as these phases passed through gases of varying composition. The perovskite observed by MACPHERSON *et al.* (1983) in the altered region of MUCH-1 may be the phase that cocondensed with hibonite. The trace element data support the textural and petrographic arguments that MUCH-1 is a condensate (MACPHERSON *et al.*, 1983).

5.4 *BB-6*

Although they could not measure the characteristic thulium anomaly with sufficient precision, EKAMBARAM *et al.* (1984) inferred that BB-6 has a group II REE pattern on the basis of the depletion of several HREE compared with LREE, a negative europium anomaly and an ytterbium enrichment factor similar to that of europium. Since this work demonstrates that nearly all hibonite is depleted in HREE relative to LREE (Figs. 1–4), these criteria alone cannot be used to identify a sample as a group II inclusion. The REE pattern of BB-6 hibonite is indeed different from that observed in hibonite believed to come from group III inclusions, DJ-1, MUCH-1 and BB-5, in that thulium is enriched relative to the neighboring erbium and there is a substantial drop in enrichment factor from samarium to gadolinium. Thus BB-6 is a group II inclusion.

BB-6 hibonite is unlike bulk group II inclusions (DAVIS and GROSSMAN, 1979) in two respects: thulium has a lower enrichment factor than the LREE and ytterbium is depleted relative to europium. The fractionated HREE patterns of DJ-1 and MUCH-1 are believed to have arisen from REE partitioning between hibonite and other condensed phases in closed systems with bulk group III REE patterns. The differences between the Tm/Sm and Yb/Eu ratios in BB-6 hibonite and those in bulk group II inclusions are probably

caused by the same process. This is consistent with the observation that in BB-6 hibonite the depletion of thulium relative to LREE (Tm/Sm_{Cl} = 0.46 ± .16) is intermediate between the depletions seen in DJ-1 and MUCH-1 (Tm/Sm_{Cl} = 0.16 ± .02 and 0.56 ± .08, respectively). BB-6 hibonite reflects some other peculiarities of group II inclusions. Group II inclusions compared with normal group I or III inclusions are enriched in volatile elements and depleted in the most refractory trace elements (GROSSMAN and GANAPATHY, 1976b; MASON and MARTIN, 1977). Similarly, BB-6 hibonite compared with hibonite from group III inclusions is enriched in volatile sodium, potassium, silicon, chromium, manganese and iron and depleted in highly refractory scandium and yttrium (Table 1, Fig. 6b). The only highly refractory element which is not significantly depleted in BB-6 hibonite is zirconium, for which the concentration is only slightly less than in hibonite from other inclusions. The reason for the lack of a significant zirconium depletion in BB-6 hibonite is unclear.

The high sodium and silicon contents of the hibonite demonstrate that enrichment of volatile elements in bulk group II inclusions is not restricted to secondary phases. Either the primary phases were initially high in volatile elements or they have been reequilibrated with a volatile-rich gas or melt at lower temperatures. Magnesium isotopic analyses show that secondary alteration in Allende coarse-grained inclusions, specifically that producing sodium-rich minerals, occurred after decay of ^{26}Al (HUTCHEON and NEWTON, 1981). BB-6 has a ^{26}Mg excess consistent with an initial $^{26}Al/^{27}Al$ ratio of $\sim 4 \times 10^{-5}$ (HUTCHEON *et al.*, 1980; HUTCHEON, pers. comm.). If sodium and silicon were introduced into hibonite, this introduction occurred before ^{26}Al decay or without magnesium isotopic exchange. Thus, it is possible that the high volatile element content of BB-6 hibonite is a primary feature.

5.5 BB-5

The bulk sample of BB-5 analyzed by EKAMBARAM *et al.* (1984, 1985) has a Cl chondrite-normalized REE pattern that resembles a group III pattern (MASON and MARTIN, 1977), but with important differences. While all group III inclusions have Yb/Yb* values very close to their Eu/Eu* values, the Yb/Yb* value, 0.031 ± .019, is only one tenth the Eu/Eu* value, 0.306 ± .090 (±2σ), in BB-5. Group III inclusions have uniform enrichments of all REE except europium and ytterbium, while BB-5 is enriched in HREE relative to LREE by a factor of ~1.3. Ion microprobe analysis of BB-5 has revealed the presence of several REE-bearing phases which can be combined to explain the bulk pattern.

Corundum is the only phase in BB-5 that does not contain REE. No LREE were detected within BB-5-C corundum; the upper limit based on a background count rate of 1 count per minute gave a total LREE content of <0.1 ppm (3σ background level) or less than 0.05 times Cl chondritic levels. HREE concentrations, although very low, may reflect minor overlap onto HREE-bearing phases described below. Scandium, titanium and vanadium appear to be present within the corundum structure, because Sc/REE, Ti/REE and V/REE ratios are much higher than one would expect from overlap onto HREE-rich phases. The concentration of titanium is far in excess of those of magnesium and iron, so titanium must exist as Ti^{3+} unless there are vacancies in the corundum structure. The concentrations of strontium, yttrium, zirconium and volatile elements in corundum are very low.

The Cl chondrite-normalized REE pattern of BB-5-1 hibonite (Fig. 1d) is similar to those of DJ-1 and MUCH-1 (Fig. 1a,b): LREE are uniformly enriched; HREE enrichments drop smoothly from gadolinium to lutetium; and superimposed on this are europium and ytterbium anomalies of similar magnitude. Levels of refractory elements other than REE in BB-5-1 hibonite are similar to those in DJ-1 and MUCH-1. Levels of volatile elements are similar to those found in DJ-1 and, except for sodium, about a factor of ten lower than in MUCH-1 (Fig. 6a).

Since BB-5-1 hibonite is depleted in HREE relative to LREE and bulk BB-5 is somewhat enriched in HREE relative to LREE, there must be additional HREE-rich phases present in this inclusion. One such phase known to be present is perovskite, which is found enclosed in hibonite (BAR-MATTHEWS *et al.*, 1982). Although the primary ion beam was larger than any of the perovskite grains in BB-5, an analysis was made centered on one of the largest ones. The minor and trace element content of this area, BB-5-2, is similar to that of pure hibonite, BB-5-1, but Fig. 2d shows that BB-5-2 has a REE pattern somewhat different from that of BB-5-1: Cl chondrite-normalized enrichments increase smoothly from lanthanum to dysprosium and then fall smoothly to lutetium. The Eu/Eu* and Yb/Yb* values in BB-5-2 are both ~0.3, in excellent agreement with BB-5-1. Dysprosium and holmium appear to have the highest enrichment factors in this perovskite, since the BB-5-2 REE pattern shows the largest excess relative to that of BB-5-1 for these REE. Hibonite in BB-5-1 and perovskite in BB-5-2 both have lower Lu/Dy ratios than BB-5 bulk, so these two components combined cannot explain the bulk BB-5 REE pattern.

The REE pattern of bulk BB-5 may be influenced by the presence of two additional HREE components that were found in submicron grains in corundum. Both components were found in one volume within corundum, BB-5-O, which gave very high concentrations of HREE, but was essentially free of LREE (Fig. 2a). In two long runs giving the REE pattern of BB-5-O, the Gd/Lu ratio was highly variable, indicating that two HREE-bearing phases were being analyzed simultaneously (Fig. 7). Areas enriched in each of the individual phases were found by searching for spots rich in either gadolinium or lutetium. The area with the lowest Gd/Lu ratio was labelled BB-5-A and the area with the highest Gd/Lu was labelled BB-5-B. Owing to the small size of HREE-rich phases in these areas and the necessity to establish quickly the major and minor element chemistry before the grain was sputtered away by the primary ion beam, REE data obtained on BB-5-A and BB-5-B are based only on single passes through the REE mass range.

Absolute abundances of REE and major elements in BB-5-A and BB-5-B (Fig. 2b) are difficult to assess due to the overlap of the primary beam onto surrounding corundum. In the lutetium-rich phase, BB-5-A, HREE increase steadily from gadolinium to lutetium. The composition of this phase was estimated by comparing its composition with that of BB-5-C corundum. If the phase contains no aluminum, spot BB-5-A contains 0.2% of a phase whose composition is ~7%

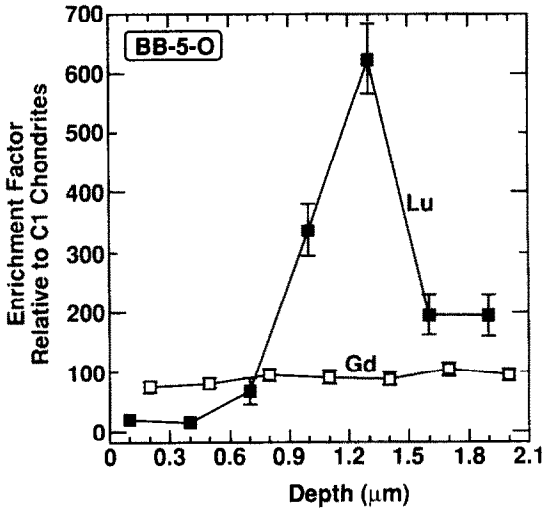

FIG. 7. Gadolinium and lutetium enrichments in BB-5-O as a function of depth within the ion microprobe hole. Gadolinium remains fairly constant, while the C1 chondrite-normalized Lu/Gd ratio varies from 0.05 to 7.1.

CaO, 7% Sc_2O_3, 13% TiO_2, 6% Y_2O_3, 65% ZrO_2 and 2% HREE oxides. This phase could be much lower in calcium, scandium and titanium if corundum in this area were slightly high in these elements. In the gadolinium-rich phase (BB-5-B) the HREE decrease from gadolinium to lutetium. BB-5-B is enriched in magnesium, calcium, titanium, yttrium and HREE relative to surrounding corundum. The Ca/Ti ratio of ~5 in BB-5-B, the presence of magnesium and the slope of the HREE pattern suggest that the gadolinium-rich phase is hibonite rather than perovskite. Comparison of the calcium content of BB-5-B with those of BB-5-1 hibonite and BB-5-C corundum indicates that BB-5-B contains 47% hibonite. The REE pattern of hibonite in BB-5-B is quite different from that of BB-5-1. If normalized to the Ca concentration of BB-5-1, BB-5-B hibonite is depleted in LREE by a factor of ~8 and enriched in HREE by a factor of ~5 compared with BB-5-1 hibonite. Both BB-5-A and BB-5-B are enriched in HREE relative to LREE. Since HREE as a group are more refractory than LREE, BB-5-A and BB-5-B can be considered to be ultrarefractory components.

The gadolinium content of BB-5-O remained fairly constant throughout the run, while lutetium was highly variable (Fig. 7). This indicates that hibonite in BB-5-O is fairly constant in composition and uniformly distributed and that zirconium-rich oxide is present as very tiny grains that are inhomogeneously distributed. The gadolinium content of BB-5-B is nearly the same as that of BB-5-O, yet the calcium content of BB-5-O is only one-seventh that of BB-5-B. The most likely explanation for this is that the calcium analysis of BB-5-O, which was done after the REE analysis, was made on a slightly different spot which contained less hibonite.

The LREE pattern of BB-5-B resembles that of BB-5-O and has substantially higher enrichments than were found in BB-5-A. The LREE patterns of the individual passes that make up the BB-5-O analysis are remarkably consistent despite the widely varying Gd/Lu ratio. Although statistically significant numbers of counts were recorded at the LREE masses, there may be molecular interferences in the LREE mass spectrum that are not completely removed by energy filtering. Nonetheless, the remarkable similarity between the shapes of LREE patterns of BB-5-O and core hibonite in GR-1 suggests that the LREE concentrations are real and indicates a similar origin for the two hibonite samples by cocondensation of hibonite and another phase with incomplete condensation of LREE (see section 5.6).

The slope of the HREE pattern of BB-5-B is similar to that of BB-5-1 hibonite, but BB-5-B is strongly depleted in LREE. Such a pattern could be explained if the volume analyzed in BB-5-B contained a hibonite grain that condensed at such a high temperature that LREE did not condense. The decreasing enrichment factor with increasing atomic number among HREE in BB-5-B hibonite requires that other phases, enriched in heavier over lighter HREE, condensed with it. One candidate for such a phase is the one present in BB-5-A, which is enriched in the heaviest HREE. BB-5-A and BB-5-B cannot be combined to give a flat HREE pattern. When they are combined, as in BB-5-O, they give a HREE pattern depleted in the middle range of HREE. The middle HREE cannot be depleted due to volatility, because they are more refractory than lighter HREE in BB-5-A and more volatile than heavier HREE in BB-5-B. The carrier for middle HREE may be perovskite, since perovskite-bearing BB-5-2 is most highly enriched in these HREE. Perovskite in the Ornans ultrarefractory inclusion OSCAR is also enriched in the middle HREE (DAVIS and HINTON, 1985). Formation of the HREE-enriched components in BB-5 probably took place by high temperature cocondensation of hibonite, perovskite and zirconium oxide. It is not clear whether perovskite is missing from the ultrarefractory assemblage within BB-5 corundum or was not observed by us or BAR-MATTHEWS *et al.* (1982).

EKAMBARAM *et al.* (1984) had difficulty explaining the large ytterbium anomaly coupled with a much smaller europium anomaly in BB-5, because during gas-solid fractionation in gases of relatively reducing solar composition (DAVIS and GROSSMAN, 1979) or in oxidizing gases (DAVIS *et al.*, 1982) ytterbium is always more refractory than europium. They suggested that BB-5 condensed as a group III inclusion with equally large europium and ytterbium anomalies and subsequently equilibrated with another phase under reducing conditions where only europium (as Eu^{2+}) was added. The REE pattern of bulk BB-5 (EKAMBARAM *et al.*, 1984, 1985) can be explained by a combination of the REE patterns of BB-5-1 hibonite and the combined HREE-rich phases within corundum, BB-5-O. The bulk BB-5 data were first normalized to the Ca concentration measured in BB-5-1 hibonite. A sufficient quantity of BB-5-O was added to BB-5-1 to match the terbium enrichment factor in the calcium-normalized bulk. Although the calculated pattern is higher in ytterbium than the bulk pattern (Fig. 2c), the calculated pattern has an ytterbium anomaly that is significantly larger than its europium anomaly. The remaining REE agree quite well in the two patterns. BB-5-A and BB-5-B, which dominate the REE pattern of BB-5-O, do not contain detectable levels of ytterbium. BB-5-O may be contaminated with a minor amount of another ytterbium-bearing phase. Nonetheless, BB-5-O was used in the mixing calculation because its REE data were more precise than those of BB-5-A and BB-5-B. If the component

mixed with BB-5-1 was HREE-rich with no ytterbium, the calculated pattern would have an ytterbium abundance that overlaps that of the bulk REE pattern. In BB-5, hibonite is depleted in the heaviest HREE and the ultrarefractory components are enriched in HREE, so addition of the ultrarefractory components to BB-5-1 deepens the ytterbium anomaly while only having a minor effect on the europium anomaly. Thus, BB-5 appears to be a mixture of hibonite typical of a group III inclusion with an ultrarefractory component enriched in HREE, but very low in LREE and ytterbium.

The two major REE-bearing portions of BB-5 have different condensation histories. The REE pattern of BB-5-O has a step between LREE and HREE while that of BB-5-1 does not. The HREE condensed into several high temperature phases, which were trapped in corundum and removed from equilibrium with the gas. BB-5-1 hibonite condensed from a reservoir which experienced no significant amount of prior removal of highly refractory HREE. It is possible that both BB-5-1 and BB-5-O formed in the same reservoir if the trapping of HREE at high temperature was inefficient. As shown for DJ-1 and MUCH-1, condensation of hibonite with a smoothly fractionated HREE-poor pattern must occur by cocondensation of another phase with a HREE-rich sloping pattern. As in DJ-1 and MUCH-1, hibonite must have been separated from the missing HREE-rich phase. There are three possibilities for this: (1) hibonite was mechanically separated from a group III inclusion prior to incorporation into BB-5; (2) perovskite or some other phase that favors HREE cocondensed with, but did not accrete with BB-5; and (3) the second phase is not missing from BB-5, but only from the sample taken for bulk analysis.

BAR-MATTHEWS *et al.* (1982) demonstrated that despite enormous variations in the Al/Mg ratio both hibonite and corundum have uniform δ^{26}Mg values of $\sim +7‰$. Both magnesium and calcium in BB-5 hibonite are isotopically mass fractionated in favor of light isotopes (Table 4). The lack of a large ^{26}Mg excess may have been caused by exchange of magnesium with an external reservoir after decay of ^{26}Al. The uniform magnesium isotopic mass fractionation makes this rather unlikely, because in other refractory inclusions where magnesium exchange is suspected, the exchange occurs with a reservoir of near-normal isotopic composition (FAHEY *et al.*, 1985d; DAVIS *et al.*, 1986; LAUGHLIN *et al.*, 1986; MACPHERSON *et al.*, 1986). The uniform ^{26}Mg excess, the lack of evidence for decay of ^{26}Al and the mass fractionated magnesium and calcium reflect formation from an isotopically peculiar reservoir. There is a second possible interpretation of the magnesium isotopic data that requires an isotopically peculiar reservoir. IRELAND (1987a) found that a number of hibonite grains from C2 chondrites show a 1:1 correlation between $-\Delta^{25}$Mg and δ^{26}Mg, generally in the direction of excess ^{26}Mg and isotopically light magnesium. He suggested that such a correlation could be produced by mixing monoisotopic ^{24}Mg normal magnesium, in much the same way that ^{16}O is mixed with normal oxygen in most refractory inclusions (R. N. CLAYTON *et al.*, 1973). Ireland's data turned out to be incorrect because of an analytical artifact (T. R. IRELAND, pers. commun.), but this still remains a possible explanation for magnesium in BB-5, because Δ^{25}Mg and δ^{26}Mg have the same magnitude and opposite sign (Table 4). The very large ^{50}Ti depletion of $-68‰$ in BB-5 (HINTON *et al.*, 1985a, 1987b) certainly requires formation in a reservoir with a peculiar titanium isotopic composition. The similarity of hibonite and corundum in their magnesium and titanium isotopic compositions indicates that both phases formed in the same reservoir. The δ^{50}Ti value calculated from the mass scan of BB-5-O made for trace element analysis, $-64 \pm 17‰$, is in good agreement with the hibonite and corundum values. Since 50–75% of the titanium in BB-5-O is contributed from HREE-rich trace phases, the latter must have formed from the same isotopic reservoir as the major phases.

The presence of a "trapped" ultrarefractory HREE component within corundum demonstrates that BB-5 cannot have been totally molten at any time. It also rules out the possibility of formation by evaporation unless corundum and small HREE-rich grains were the only refractory residue. The most plausible scenario is a formation by condensation with limited time available for reequilibration as the temperature fell. Condensation must have occurred from a reservoir with isotopically anomalous titanium and magnesium and lacking ^{26}Al. Fractionation in both calcium and magnesium may have been caused by a single condensation process; however, the large degree of mass fractionation suggests that this is unlikely.

5.6 GR-1

GR-1 has a concentric structure, with a hibonite core, a corundum mantle and a hibonite rim. MACPHERSON *et al.* (1984) found significant differences in mineral chemistry between rim and core hibonite in this inclusion. These hibonite regions are also quite different in their trace element and isotopic compositions (Fig. 3, Tables 1, 2 and 4), not only from each other, but from other hibonite analyzed in this work.

Rim hibonite (GR-1-R) is higher in magnesium than core hibonite, but significantly depleted in refractory elements compared to core hibonite and Murchison hibonite in general. Core hibonite gave variable contents of zirconium and yttrium due to overlap of the primary ion beam onto a refractory oxide phase at the boundary between core hibonite and mantle corundum (see photomicrograph in MACPHERSON *et al.*, 1985). The low ends of the ranges given in Table 1 for yttrium and zirconium are believed to be representative of core hibonite. The zirconium content of rim hibonite is ~ 2 times lower than that of core hibonite and ~ 10 times lower than those of other Murchison hibonite. Core hibonite (GR-1-C) is enriched in scandium relative to rim hibonite (Fig. 6c), but this enrichment cannot be due to the refractory oxide grains surrounding the core. The atomic Zr/Sc ratio in these grains is ~ 1 (MACPHERSON *et al.*, 1984) while that in core hibonite is $\sim 7 \times 10^{-3}$. Overlap of the beam onto this phase would result in much larger zirconium contents than are observed. The strontium and barium contents of core hibonite are similar to those of other Murchison hibonite reported here, but rim hibonite is substantially depleted in these elements (Fig. 6c). Strontium and barium are among the most volatile of the elements normally considered refractory.

In some areas of GR-1 core hibonite, count rates at $m/e = 176$ to 192 were observed that are in excess of those that attributable to LnO^+ ions of HREE. Especially high count

rates were observed at m/e = 188, 189, 190 and 192. Relative proportions of these peaks match the isotopic composition of osmium quite well, so we conclude that osmium is present. The count rates at m/e = 191 and 193, corresponding to iridium, are much lower. This is not surprising, because the ion yield of Ir^+ under oxygen bombardment of iridium metal is only one tenth that of Os^+ from osmium metal (STORMS *et al.*, 1977). The ratio of the count rate at m/e = 192 to that at m/e = 139, which should be proportional to the Os/La ratio, varied between 0.02 and >100. Since osmium is always accompanied by other refractory siderophile elements, refractory nuggets appear to be heterogeneously distributed within core hibonite.

GR-1 core and rim hibonite have very different REE patterns (Fig. 3). They contain the highest and lowest REE concentrations, respectively, of all hibonite analyzed in our laboratory. The C1 chondrite-normalized LREE pattern in core hibonite is very irregular and there is a distinct break between samarium and gadolinium. LREE are depleted by factors of 3.5 to 8.9 compared to gadolinium. HREE decrease monotonically from gadolinium to erbium, then fall sharply to thulium. Europium and ytterbium are strongly depleted relative to neighboring REE. Although the ytterbium concentration could not be measured, due to large interfering GdO^+ peaks, there is clearly a significant depletion. The cosmochemical behavior of yttrium is similar to that of the HREE: it is trivalent and has an ionic radius between those of dysprosium and holmium; its refractoriness is similar to those of erbium and lutetium. The Y/Zr ratio in the refractory oxide phase between core hibonite and the mantle corundum (MACPHERSON *et al.*, 1984) is ~1. The very high Y/Zr ratio core hibonite (Table 1) implies that the bulk of the REE are in solid solution in hibonite rather than concentrated in zirconium-rich oxide grains. Some variations of the slope of HREE patterns were observed from run to run: C1 chondrite-normalized Lu/Gd ratios vary from 0.03 to 0.19. In contrast, LREE patterns were constant. The slopes in HREE patterns of core hibonite are correlated with zirconium content and probably reflect overlap onto zirconium-rich grains. These grains appear to be more lutetium-rich than hibonite, as was observed in BB-5.

REE concentrations are much lower in rim hibonite (GR-1-R) than in core hibonite (GR-1-C). Rim hibonite grains are quite small, so the beam spot overlapped onto corundum. Although uncertainties are given for LREE in rim hibonite, the concentrations should be considered as upper limits because of molecular interferences, a possibility raised by the low levels and irregular pattern of the LREE. HREE are substantially more enriched than LREE in rim hibonite. The C1 chondrite-normalized Dy/Ce ratio is ≥11 in the rim compared to 6 for the core. Rim hibonite differs from core hibonite in having much less fractionation among HREE.

REE concentrations in GR-1 corundum (GR-1-M) are extremely low. Although concentrations listed in Table 2 are usually larger than 2σ uncertainties, we cannot exclude the possibility that the observed count rates are due to molecular interferences. Therefore, these values should be considered as upper limits.

Magnesium and calcium isotopic compositions were measured for both core and rim hibonite. HINTON *et al.* (1987b) measured the titanium isotopic composition of these hibonite areas. Magnesium in both core and rim hibonite is mass fractionated in favor of the light isotopes by about 5‰/amu (Table 4). Initial magnesium isotope measurement (HINTON *et al.*, 1984a) suggested an apparent δ^{26}Mg value of −3‰ in both core and rim. Further analyses did not confirm this depletion; no ^{26}Mg anomalies greater than 2σ are observed in GR-1 hibonite (Table 4). HINTON *et al.* (1984a) combined measurements of calcium mass fractionation for both core and rim hibonite to give a Δ^{44}Ca value of ~−5‰/amu. Further analyses showed that while both core and rim hibonite are fractionated in favor of light isotopes, rim is much lighter (−7.3 ± 1.4‰/amu) than the core (−2.6 ± 1.9‰/amu). This difference of nearly 5‰/amu in calcium mass fractionation between two portions of the inclusion is quite large. The entire range of Δ^{44}Ca observed by NIEDERER and PAPANASTASSIOU (1984) in Allende refractory inclusions is from −2.3 to +1.8‰/amu (with the exception of HAL and B-29). The amount of fractionation observed between GR-1 core and rim hibonite is too large to be explained by a single stage fractionation process. More likely, the two generations of hibonite formed in two different isotopic reservoirs. The reservoirs may be related through multistage condensation and evaporation steps.

DAVIS and GROSSMAN (1979) showed that although calculations of REE condensation in a gas of solar composition indicated small differences in volatility between the LREE, uncertainties in thermodynamic data also allow the possibility that lanthanum, cerium, praseodymium, neodymium and samarium have exactly the same volatility. When these authors modeled gas-solid fractionation of REE in attempting to explain group II REE patterns, they assumed that the LREE all had the same volatility, because most group I, II and III REE patterns have nearly uniform abundances of LREE. Since GR-1-C is enriched in HREE over LREE, the LREE are probably incompletely condensed and the irregular LREE pattern may be caused by the relative volatilities of the LREE.

We have applied calculations of gas-solid partitioning behavior of the LREE to GR-1 core hibonite, using methods described in DAVIS and GROSSMAN (1979). A calculation was done for a gas of solar composition at a total pressure of 10^{-3} atm at 1710 K. Thermodynamic data for gaseous REE monoxides were taken from PEDLEY and MARSHALL (1983); data for all other compounds were the same as in DAVIS *et al.* (1982). Hibonite clearly shows nonideal solid solution of lanthanides. In order to calculate the depletion of LREE due to volatility, one must first estimate what the REE pattern of the hibonite would have been if there were no LREE depletion. The HREE pattern of GR-1-C hibonite resembles that of other hibonite analyzed here in having a monotonic decrease in REE enrichment factor from gadolinium to lutetium (except for ytterbium). This type of pattern is believed to be caused by partitioning of REE between hibonite and perovskite or another refractory oxide. The slope of the HREE pattern in GR-1-C is intermediate between those of HAL and DJ-1. Had the LREE completely condensed, GR-1-C would have a LREE pattern with a slope intermediate between those of HAL (except for cerium and praseodymium) and DJ-1. We estimate that it would follow the HREE and smoothly extrapolate to a C1 chondrite-normalized enrich-

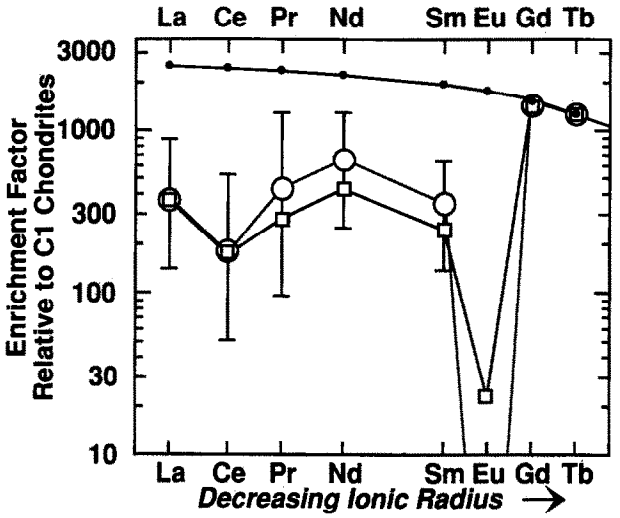

FIG. 8. C1 chondrite-normalized enrichment factors of LREE in GR-1-C compared with calculated abundances of LREE in hibonite in a gas of solar composition at 1710 K. Open squares represent the measured pattern of GR-1-C; small solid circles represent the LREE pattern that GR-1-C would have had if the LREE had fully condensed into hibonite and its competitors; and large open circles with error bars represent LREE abundances calculated from thermodynamic data. Uncertainties shown are the ranges of LREE patterns allowed by uncertainties in thermodynamic data. Despite uncertainties in thermodynamic data, there is an excellent match between the calculated and observed patterns.

ment factor of 2500 for lanthanum (Fig. 8). The deviation of this estimated pattern from a flat one takes into account nonideal solid solution behavior and competition with other cocondensing REE-bearing phases. It is an estimate of what the REE pattern of GR-1-C would have looked like at a temperature low enough (~1600 K at a solar nebular pressure of 10^{-3} atm) that the LREE had fully condensed. The fraction of each REE condensed into a single model host phase was calculated at 1710 K using an activity coefficient of 1 for all REE. Assuming that REE activity coefficients in hibonite and the identities and amounts of cocondensing REE-bearing phases do not vary significantly with temperature, then the distribution coefficient of REE between hibonite and cocondensing phases is approximately the same at 1710 K as at 1600 K. In order to take into account the effect of partitioning of REE on the shape of the REE pattern of condensate hibonite at 1710 K, the calculated pattern of the model host phase was then multiplied by the enrichment factors in the above-estimated GR-1-C pattern and compared with observed enrichments in GR-1-C (Fig. 8). Uncertainties in thermodynamic data still permit all LREE to have the same volatility, but there is a remarkable similarity between the LREE pattern in GR-1 core and the calculated pattern. We conclude that the variations in LREE enrichments in GR-1 core hibonite are due to small differences in volatility of LREE.

Although gas-solid partitioning can explain depletion of LREE relative to HREE in GR-1 core hibonite, the europium concentration is much greater than expected from volatility considerations. A separate addition of volatile europium must have occurred prior to formation of rim hibonite, as the latter is ten times lower in europium than the core.

We have inferred that GR-1 core hibonite would have been enriched in lanthanum by a factor of ~2500 compared to C1 chondrites if lanthanum had fully condensed into hibonite and its REE-bearing cocondensates. This implies that only one part in 2500 of the total condensable matter had condensed into this hibonite when it formed. If aluminum were fully condensed in the form of hibonite, a trace element refractory enough to fully condense into this hibonite would have an enrichment factor of 58, using C1 chondritic abundances slightly modified from those of ANDERS and EBIHARA (1982). In the condensation sequence given by DAVIS *et al.* (1982), corundum condenses at 1742 K and is replaced by hibonite at 1727 K in a gas of solar composition at $P_{tot} = 10^{-3}$ atm. Since there is negligible solid solution of REE and most other refractory trace elements in corundum, these elements only begin to condense when hibonite begins to form from corundum. If GR-1-C hibonite formed by this mechanism, it must have been separated when only 58/2500 (2.3%) of the hibonite that could possibly form had actually formed. The temperature at which this fraction of hibonite condenses at $P_{tot} = 10^{-3}$ atm is 1726.88 K, only 0.09 K below the temperature at which hibonite appears. The fractionated HREE pattern of GR-1-C hibonite implies that the REE were partitioned between hibonite and at least one other phase. Perovskite is not believed to be the second phase, because its condensation temperature is 1676 K at $P_{tot} = 10^{-3}$ atm, below the temperature range inferred for formation of GR-1. Zirconium-rich oxide is suspected, as this phase is enriched in the heaviest HREE in BB-5. Zirconium oxide first condenses at 1808 K and is 90% condensed at 1730 K in a gas of solar composition at $P_{tot} = 10^{-3}$ atm, so it is reasonable to assume that it had already condensed when hibonite formed by reaction of the gas with corundum. If hibonite is 2.3% condensed and zirconium oxide is fully condensed, the hibonite/zirconium oxide weight ratio calculated from cosmic abundances is ~100. Given what is known about the partitioning behavior of these two phases, most of the LREE are likely to be in hibonite and most of the heaviest HREE are likely to be in zirconium oxide. Lutetium should be largely condensed into zirconium oxide at 1730 K. Based on C1 chondritic abundances, the enrichment factor of lutetium in zirconium oxide should be $\sim 2 \times 10^5$ and the concentration of Lu should be ~5000 ppm. Under ideal solid solution, the light REE are only 0.1% condensed at this temperature, yet in GR-1-C hibonite, they appear to be ~15% condensed. In order for the LREE to be this refractory, the activity coefficients for lanthanum and other LREE in hibonite must be quite low, ~0.02.

The above derivation of the activity coefficients for LREE in hibonite depends on many assumptions and illustrates the difficulty in determining absolute activity coefficients from natural inclusions. DRAKE and BOYNTON (1988) have calculated absolute activity coefficients for REE in hibonite from hibonite-liquid partitioning experiments made under a variety of oxygen fugacity conditions. Their inferred activity coefficients range from 330 for lanthanum to 24,000 for ytterbium. Their derivation also involved many assumptions and gave activity coefficients more than four orders of magnitude larger

than ours. Although the relative activity coefficients of DRAKE and BOYNTON may be correct, the absolute ones are almost certainly too high. Proceeding with their assumption that the activity coefficients of trivalent REE in silicate liquids are all about the same, 2400, the activity coefficients for solid solution of lanthanum in perovskite and melilite are 1100 and 4800, respectively. If REE activity coefficients are of this order of magnitude and REE condensation occurs by solid solution in major condensate phases, lanthanum and the other LREE would not be refractory elements. 80% of the lanthanum would still be in the gas phase at the temperature at which most refractory inclusions are thought to have ceased equilibrating with the gas, ~1470K at $P_{tot} = 10^{-3}$ atm. The pure lanthanide oxides are quite refractory compounds and are expected to condense on their own if solid solution in major phases is thermodynamically unfavorable; similarly, lanthanide oxides might be expected to appear as a separate phase in the partitioning experiments of DRAKE and BOYNTON (1988) if REE are strongly excluded from other liquid and crystalline phases. Since lanthanide oxides are not observed in refractory inclusions or in partitioning experiments, activity coefficients for REE in hibonite and other phases must be much lower than they inferred and could be less than one for hibonite and perovskite.

Zirconium-rich grains occur between GR-1-C hibonite and GR-1-M corundum. A rastered beam analysis of bulk GR-1 was made (GR-1-B in Tables 1 and 2). Although not plotted, the trace element pattern resembles that of core hibonite. Either zirconium oxide is underrepresented in the plane of the polished section or zirconium oxide and hibonite cocondensed and were separated prior to assembly of GR-1.

One possibility advanced by MACPHERSON *et al.* (1984) for the presence of two generations of hibonite in GR-1 was that pure hibonite was flash-heated such that some hibonite incongruently melted to corundum and a calcium-rich liquid. Calcium was then preferentially volatilized from the melt. Upon cooling, a second generation of hibonite crystallized at the outside of the inclusion. The core hibonite was viewed by MACPHERSON *et al.* (1984) as an unmelted relict grain. If GR-1 were once pure hibonite, a loss of >80% of the calcium would be required to produce the observed proportions of hibonite and corundum; however, it is difficult to believe that relict hibonite could survive under these conditions. In nonideal solution of REE in hibonite, all REE except europium and ytterbium are calculated to be more refractory than calcium. Since calcium loss should be more complete than REE loss from the melt, the liquid would be more enriched in REE than the original hibonite. Thus, the extremely low refractory trace element content of GR-1 rim hibonite makes it unlikely that the rim is a late-stage crystallization product from an aluminum-rich melt. Hibonite low in refractory trace elements is more likely to have formed by reaction of the exposed corundum with solar nebular gas at lower temperature after REE had condensed but while some calcium was still available in the gas. The different calcium isotopic mass fractionation in core and rim hibonite indicates that formation of rim hibonite took place in a different isotopic reservoir than that in which core hibonite and mantle corundum formed. This second possibility was also mentioned by MACPHERSON *et al.* (1984).

5.7 *HAL and DH-H1*

Hibonite-normalized trace element enrichment patterns of HAL and DH-H1 show a remarkable degree of fractionation from more normal hibonite patterns (Fig. 6). The most dramatic effects are substantial depletions in vanadium and cerium. Fractionations compared with normal hibonite are generally more extreme in DH-H1 than in HAL hibonite: DH-H1 is even more depleted in cerium and vanadium and is depleted in barium whereas HAL hibonite has close to normal levels of this element. DAVIS *et al.* (1982) performed extensive calculations on gas-solid fractionation of trace elements in a variety of oxygen partial pressures and found that cerium and vanadium become much more volatile and barium somewhat more volatile than other refractory elements in oxidizing environments. They attributed low cerium, vanadium and barium contents of HAL hibonite to the oxidizing environment in which HAL formed. We find, however, that hibonite in general is less enriched in barium than in many other refractory lithophile elements (Fig. 5) and that HAL hibonite is similar in barium content to other more normal hibonite, such as MUCH-1, DJ-1 and BB-5-1 (Fig. 6). The general depletion of barium probably occurs because it is one of the least refractory of the lithophiles normally considered refractory in a gas of solar composition. The large ionic radius of Ba^{2+} may also cause it to favor other host phases compared to hibonite. Thus, depletion of barium relative to other refractory lithophiles in hibonite compared with C1 chondrites cannot be attributed to oxidizing conditions during formation. The depletion of barium in DH-H1 compared to HAL and other hibonite, as well as the larger depletions of cerium and vanadium, may indicate that DH-H1 formed under more oxidizing conditions than HAL.

REE patterns of the two hibonite samples are similar (Fig. 4); however, cerium is depleted relative to lanthanum in DH-H1 by a factor of 1770 ± 770 relative to C1 chondrites, a depletion three times larger than that in HAL hibonite, 543 ± 123. The slope of the REE pattern of DH-H1 is also steeper than that of HAL (C1-normalized La/Ho ratios of 21 and 12, respectively). The sizes of the cerium depletions in HAL and DH-H1 hibonite approach the limit of ~2000 set by thermodynamic data for condensation or evaporation under oxidizing conditions (DAVIS *et al.*, 1982). From their Fig. 3, the cerium depletion in DH-H1 hibonite indicates formation at $P_{tot} < 10^{-12}$ atm in a C1 chondritic gas or in ejecta from helium- or carbon-burning zones of supernovae with C/O < 1. There is another possible explanation for at least part of the depletion of cerium in these hibonite samples. DAVIS and HINTON (1986) determined REE patterns in coexisting perovskite and hibonite in a tiny Ornans refractory inclusion and found that hibonite has a negative cerium anomaly and perovskite a positive one. They suggested that under oxidizing conditions, where most lanthanides are trivalent but cerium is tetravalent, Ce^{4+} might more easily substitute into perovskite and thus be partitioned differently than neighboring REE. If lanthanides partitioned between hibonite and perovskite in both HAL and DH-H1 during condensation under highly oxidizing conditions, and Ce^{4+} is more enriched in perovskite than in hibonite, the latter could have a cerium anomaly larger than that calculated assuming identical solid

solution behavior for La^{3+}, Ce^{3+} and Ce^{4+}, as was done by DAVIS *et al.* (1982). The difference in partitioning of cerium and other REE between hibonite and perovskite could also explain why the cerium depletion factor measured by DAVIS *et al.* (1982) in the perovskite-rich rim layers of HAL is not as large as those observed for the hibonite core.

The FeO contents of DH-H1 and HAL hibonite, 0.44 and 0.63 wt% (Table 1), respectively, are much higher than in Murchison hibonite, ≤0.05 wt% (MACPHERSON *et al.*, 1983, 1984). As noted by ALLEN *et al.* (1980), the higher iron contents probably reflect the oxidizing conditions under which the HAL and DH-H1 hibonite formed. HAL hibonite is unusual in having fewer atoms of magnesium than titanium per formula unit. Fe^{2+} may partially replace Mg^{2+} in the coupled substitution $Mg^{2+} + Ti^{4+} = 2\ Al^{3+}$. DH-H1 hibonite has an unusually low Ti concentration of 541 ppm, a factor of ~8 lower than HAL hibonite. The atomic (Fe + Mg)/Ti ratio is 5.5. As no other tetravalent cations are present in amounts sufficient to balance divalent iron, Fe^{3+} may be present. This provides support for the hypothesis that DH-H1 formed under more oxidizing conditions than HAL.

Concentrations of the volatile elements manganese and chromium are dissimilar in the two hibonite samples. Manganese is slightly lower in DH-H1 hibonite than in HAL hibonite, but is still somewhat higher than in Murchison hibonite samples DJ-1, BB-5 and GR-1. Chromium is significantly higher in DH-H1 hibonite than in most other hibonite analyzed. BB-6 is also high in chromium, but it is also higher in other volatile elements than is DH-H1. The major condensation reaction for chromium is: $2Cr_{(g)} + 3O_{(g)} = Cr_2O_{3(s)}$, while that for most lanthanides and aluminum is: $2MO_{(g)} + O_{(g)} = M_2O_{3(s)}$. As conditions become more oxidizing, the condensation reaction for chromium is driven to the right more rapidly than is that for aluminum and most lanthanides. Thus, the higher chromium content may indicate that DH-H1 hibonite formed under more oxidizing conditions than HAL and other hibonite. A more mundane explanation of the high chromium content is that there was overlap of the beam onto the chromium-rich spinel surrounding DH-H1 hibonite.

In DH-H1 praseodymium is strongly depleted relative to neodymium, in contrast with the slight depletion observed in HAL and the lack of depletion in DJ-1, MUCH-1, BB-6 and BB-5 (Figs. 1 and 4). The praseodymium depletions in DH-H1 and HAL hibonite suggest that $PrO_{2(g)}$ may be an important species in gas-solid fractionation under oxidizing conditions. If so, praseodymium could become more volatile than lanthanum and neodymium in oxidizing environments by the same mechanism thought to be responsible for enhanced volatility of cerium (BOYNTON and CUNNINGHAM, 1981; DAVIS *et al.*, 1982). No reliable thermodynamic data exist for $PrO_{2(g)}$ or $PrO_{2(s)}$, although $PrO_{2(g)}$ has been observed during Knudsen cell evaporation of $Pr_2O_{3(s)}$ (STALEY and NORMAN, 1969). FEGLEY (1986) calculated REE volatilities under oxidizing conditions, using thermodynamic data for a number of gaseous REE dioxides. In addition to cerium depletions, depletions in neodymium and gadolinium were predicted. Since depletions in these elements are not seen in DH-H1 hibonite, the sample with the largest negative cerium anomaly measured to date, we concur with FEGLEY's (1986) suggestion that the data used for gaseous REE dioxides are probably not reliable.

The similarity of the sloping REE patterns of HAL and DH-H1 and the presence of sloping HREE patterns in other hibonite samples strongly suggests that the REE patterns were generated by partitioning of REE between hibonite and another solid or liquid phase. The phase which competed with hibonite for REE in HAL was probably perovskite, since abundant perovskite was observed in friable rim layers which surround the core hibonite (ALLEN *et al.*, 1980). INAA analyses of the rim layers (DAVIS *et al.*, 1982) gave C1 chondrite-normalized REE patterns showing enrichments in HREE. Relative partition coefficients for REE between hibonite and perovskite were estimated from analyses of coexisting phases in the Murchison inclusion SH-7 (HASHIMOTO *et al.*, 1986; unpublished data from this laboratory), assuming local equilibrium. Using these partition coefficients we have modeled HAL to test the hypothesis that the REE patterns in core hibonite and rim in HAL are due only to partitioning between hibonite and perovskite. In this calculation we assume that partitioning occurs in a reservoir with uniform REE enrichment factors relative to C1 chondrites and that all REE in friable rim layer 4 are contained in perovskite. Using measured contents of lanthanum and dysprosium in hibonite and samarium in the friable rim layer, we calculated the proportions of hibonite and perovskite in HAL, the enrichment factor for all REE in bulk HAL (hibonite plus friable rim layer 4), absolute partition coefficients between hibonite and perovskite and complete REE patterns for hibonite and friable rim layer 4 in HAL. The calculated and observed REE patterns of hibonite are in excellent agreement (Fig. 9). The calculated pattern for friable rim layer 4 is also close to the observed pattern, but is slightly lower in lanthanum and higher in the heaviest HREE. The calculation supports the idea that perovskite is the major REE carrier in the friable rim layers. The observed enrichment factors for cerium in hibonite and rim layer 4 are much lower than the respective calculated values and the observed enrichment factor for praseodymium in hibonite is slightly lower than the calculated value, because the reservoir was not assumed to have cerium and praseodymium anomalies. FAHEY *et al.* (1987b) measured REE in a sample of the black rim surrounding HAL hibonite and showed that it had a similar pattern to friable rim layer 4, but with lower absolute enrichment factors. This pattern also has a praseodymium depletion relative to the value expected from the calculations. Perovskite and hibonite in HAL appear to have condensed together from an oxidizing gas and were removed from the gas when little of the cerium had condensed and about 75% of the praseodymium had condensed.

DH-H1 hibonite has a similar REE pattern to HAL hibonite and may also have coexisted with perovskite. The steeper REE pattern of DH-H1 hibonite can be modeled if the ratio of hibonite to perovskite when REE partitioning took place was approximately 35% of that in HAL. Perovskite was not observed surrounding DH-H1 hibonite. If it once coexisted with the hibonite, it must have been lost.

In addition to its more deviant chemical properties, DH-H1 also shows larger deviations from normal isotopic composition than does HAL (Table 4). Calcium in DH-H1 is

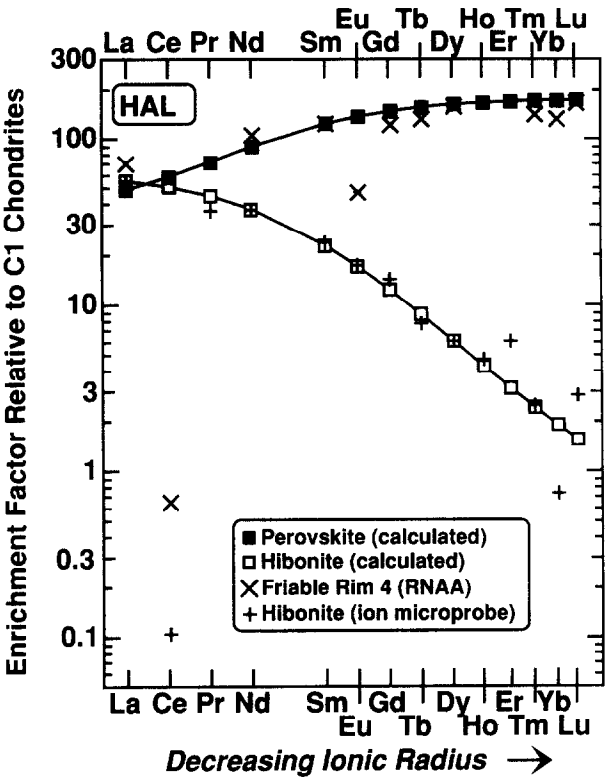

FIG. 9. Enrichment factors relative to C1 chondrites calculated for coexisting hibonite and perovskite compared to enrichment factors measured for HAL hibonite by ion microprobe and for the most REE-rich of the friable rim layer samples analyzed by RNAA (DAVIS *et al.*, 1982).

strongly mass fractionated in favor of heavy isotopes, with a $\Delta^{44}Ca$ value almost twice that of HAL. Titanium is mass fractionated in HAL hibonite by 5 ± 1‰/amu and contains a distinct positive ^{50}Ti anomaly ($\delta^{50}Ti = +14.0‰$, FAHEY *et al.*, 1987a). Although the low titanium content prohibited measurement of the $^{47}Ti/^{49}Ti$ ratio in DH-H1 under low mass resolution conditions in the Chicago ion microprobe, A. J. FAHEY and E. ZINNER (pers. commun.) were able to do so using a Cameca IMS-3F ion microprobe. They found that titanium in DH-H1 is enriched in the heavy isotopes by ~11‰/amu. In contrast to the unfractionated magnesium in HAL hibonite, magnesium in DH-H1 is fractionated in favor of heavy isotopes by 19‰/amu (HINTON and BISCHOFF, 1984). The initial $^{26}Al/^{27}Al$ ratio determined for DH-H1 hibonite, 8.6×10^{-6} (HINTON and BISCHOFF, 1984), is distinctly lower than the ratio commonly observed in refractory inclusions, 5.1×10^{-5}. Recent measurements of HAL hibonite (FAHEY *et al.*, 1987a) give a slight ^{26}Mg excess, indicating an initial $^{26}Al/^{27}Al$ ratio of $(5.2 \pm 1.7) \times 10^{-8}$ ($\pm 2\sigma$).

Both HAL and DH-H1 hibonite formed from isotopically peculiar gases under highly oxidizing conditions. The aggregate structure of HAL (ALLEN *et al.*, 1980) make condensation a more likely origin than evaporation. DH-H1 appears to have formed under even more highly oxidizing conditions than HAL. It also shows more extreme isotopic mass fractionation of calcium and titanium. The processes responsible for the oxidizing conditions may also be responsible for the isotopic mass fractionation, but the nature of the relationship is not clear.

5.8 *General properties of trace element patterns in hibonite*

All hibonite samples analyzed in this work show depletions in HREE that can be attributed to REE partitioning between hibonite, which favors LREE, and other condensed phases, which favor HREE. Most hibonite REE patterns measured by FAHEY *et al.* (1987a) show this effect, too. The rarity of unfractionated REE patterns in hibonite implies that hibonite rarely condenses without other REE carriers. The condensation sequence of refractory phases in a gas of solar composition at a total pressure of 10^{-3} atm is as follows: zirconium oxide—1808 K; corundum—1742 K; hibonite—1727 K; perovskite—1675 K. If equilibrium condensation does occur, zirconium oxide is likely to be present when hibonite forms by reaction of the gas with corundum. As condensation proceeds to lower temperatures, perovskite is likely to condense and compete with hibonite for REE. Hibonite could only form in the absence of other REE carriers if zirconium oxide were unable to nucleate on its own. A further requirement for an unfractionated REE pattern in hibonite is that hibonite must be isolated from the gas before perovskite condenses. A number of condensation calculations suggest removal of hibonite from the gas shortly after condensation begins (SH-2 in EKAMBARAM *et al.* (1984) and GR-1 in this work), so it may not be uncommon to isolate hibonite in the 50 K interval between the hibonite and perovskite initial condensation temperatures. If hibonite forms by evaporation of less fractionated material, other phases are likely to be present with hibonite. Thus, the rarity of unfractionated REE patterns in hibonite is to be expected, regardless of whether hibonite has a condensation or evaporation origin.

5.9 *Relationships between mineralogy, chemistry and isotopic composition*

FAHEY *et al.* (1987a) noted some relationships between titanium isotopic composition and type of REE pattern. They found that all hibonite from group III inclusions has a large positive or negative ^{50}Ti anomaly. The two group III inclusions for which HINTON *et al.* (1987b) measured titanium isotopes, DJ-1 and BB-5, both show significant ^{50}Ti anomalies. FAHEY *et al.* (1987a) found that no hibonite from group II inclusions has a significant ^{50}Ti anomaly. Unfortunately, BB-6 was too small to be analyzed for titanium isotopes. FAHEY *et al.* (1987a) noted that preliminary data for GR-1 (HINTON and DAVIS, 1986b) showed evidence for an ultrarefractory REE pattern; yet, GR-1 does not have a significant ^{50}Ti anomaly. BB-5, however, also contains ultrarefractory components and has the largest ^{50}Ti deficit seen to date.

There are also some relationships between calcium isotopic mass fractionation and chemistry. The two inclusions with the most isotopically heavy calcium, HAL and DH-H1, show evidence for formation in a highly oxidizing environment. The two inclusions with the most isotopically light calcium, BB-5 and GR-1, are the only two inclusions which contain corundum and are the only two inclusions that show evidence for formation at temperatures so high that the LREE have not completely condensed.

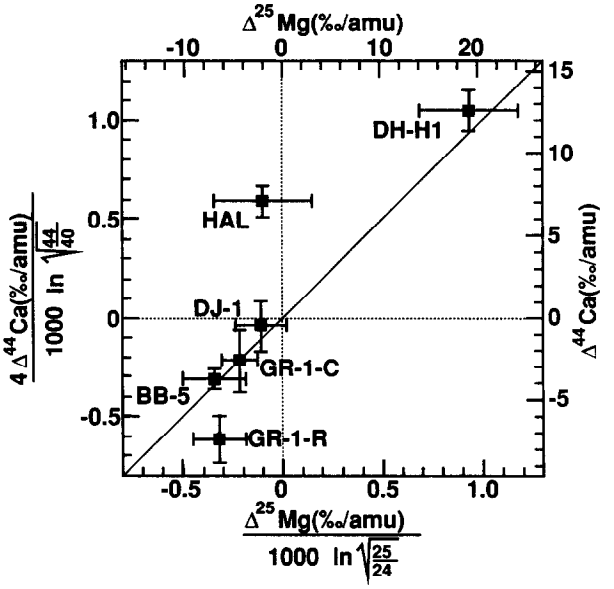

FIG. 10. Isotopic mass fractionation for calcium *vs.* that for magnesium. The uncertainties shown are $\pm 2\sigma$, based on counting statistics. Positive numbers imply enrichment in heavy isotopes. In the samples analyzed in this work, isotopic mass fractionations in calcium always have the same sign as those in magnesium.

Mass fractionations of calcium and magnesium appear to be related. In Fig. 10 are plotted calcium and magnesium fractionations normalized by the inverse square root of the mass ratios. In this representation, fractionation by the kinetic isotope effect will lie along a line of slope one if the masses involved in the fractionation are the same as those used to calculate mass ratios. We have chosen to use the masses of elemental magnesium and calcium, because the major gas phase species under solar nebular conditions are Ca and Mg. Four of the six hibonite samples analyzed lie along the slope-one line. The two samples not on the line have Δ^{25}Mg values closer to normal than would be expected for their Δ^{44}Ca values. This deviation is in the direction expected for magnesium exchange with a reservoir of near-normal isotopic composition.

FAHEY *et al.* (1987a) found that hibonite from refractory inclusions in C2 and C3V chondrites rarely contains radiogenic ^{26}Mg from decay of ^{26}Al. They also noted that there was no correlation between ^{50}Ti anomalies and radiogenic ^{26}Mg. We find that radiogenic ^{26}Mg and large ^{50}Ti anomalies are mutually exclusive. In their review of the isotopic compositions of meteoritic samples of all sorts, R. N. CLAYTON *et al.* (1988) pointed out that of all refractory inclusions containing ^{50}Ti anomalies of 10‰ or larger (and all but one with 2‰ or larger), only one, HAL (FAHEY *et al.*, 1987a), shows evidence for radiogenic ^{26}Mg. Lance HH-1, a very ^{50}Ti-poor inclusion, contains excess ^{26}Mg, but it does not appear to be correlated with Al/Mg and may not be radiogenic (FAHEY *et al.*, 1986b). Anomalies in the neutron-rich isotopes of calcium, titanium and chromium almost certainly originated in supernovae (HARTMANN *et al.*, 1985). ^{26}Al can be produced in a variety of sources, including novae (D. D. CLAYTON and LEISING, 1987), red giant stars (CAMERON, 1984), massive stars (DEARBORN and BLAKE, 1984, 1985) and supernovae (CAMERON and TRURAN, 1977). Since radiogenic ^{26}Mg and anomalies in the neutron-rich isotopes of calcium, titanium and chromium seem to be mutually exclusive in refractory inclusions, the two almost certainly were not produced in the same astrophysical source.

In the model of HINTON *et al.* (1987b) for explaining the range in ^{50}Ti anomalies in meteoritic hibonite it was proposed that there were two end members: one similar to BB-5 with a 7% deficit in ^{50}Ti and one with a large excess, of at least 10%, in ^{50}Ti. One implication of this model is that most solar system material obtained 7% of its ^{50}Ti by addition of the ^{50}Ti-rich component. Since radiogenic ^{26}Mg is never found in objects with large ^{50}Ti anomalies, ^{26}Al must have been added only to the material that had exactly 7% of its ^{50}Ti added. The material with 7% ^{50}Ti addition may have arisen from homogenization of material with a variety of ^{50}Ti anomalies, but ^{26}Al cannot have been present until after the homogenization.

The data on ^{50}Ti, ^{48}Ca and ^{54}Cr anomalies in Allende FUN inclusions C1 and EK-1-4-1 (NIEDERER and PAPANASTASSIOU, 1984; NIEDERER *et al.*, 1985; PAPANASTASSIOU, 1986) and on ^{50}Ti and ^{48}Ca in hibonite-rich inclusions (ZINNER *et al.*, 1986) provide some clues about the properties of the component containing the neutron-rich isotopes. Anomalies in these three isotopes are of comparable magnitude, in agreement with predictions of HARTMANN *et al.* (1985) for nucleosynthesis near the mass cut of a supernova. D. D. CLAYTON (1981a, 1987) has pointed out that if material from this region of a supernova condenses, it should do so as a metallic alloy, because there are essentially no elements lighter than calcium present. D. D. CLAYTON (1987) noted that it may be difficult for this condensation to occur because of the energy input from radio emission from the supernova remnant and from β^+ decay of ^{56}Ni within the zone containing the neutron-rich isotopes. He proposed that this material condensed later as tiny particles. These particles were then sputtered and redeposited onto larger oxide-rich condensates from the outer, ^{50}Ti-, ^{48}Ca-, ^{54}Cr-poor portion of the supernova ejecta which was of approximately chondritic composition. Melting and evaporation of these grains during solar system formation then produced the FUN inclusions and anomalous hibonite. Calcium and titanium are refractory elements that are enriched by about 20 times relative to C1 chondrites in all C3V refractory inclusions including the FUN inclusions. Chromium is much less refractory, with C1 chondrite-normalized enrichment factors of 0.03 to 1.5 (GROSSMAN and GANAPATHY, 1976a). If metal rich in the neutron-rich isotopes of calcium, titanium and chromium mixed with normal refractory inclusions to make FUN inclusions, one would expect the ^{54}Cr anomaly to be much larger than the ^{48}Ca and ^{50}Ti anomalies, because the mixing ratio of anomalous to normal material would be much higher for chromium than it would be for calcium and titanium. The fact that the anomalies are of comparable size implies that mixing of the neutron-rich isotopes occurred with material having roughly chondritic proportions of chromium, calcium and titanium.

In earlier cosmic chemical memory models, D. D. CLAYTON (1978, 1981a) predicted relationships between the present chemistry of refractory inclusions and their isotope anomalies.

In his model for separation of supernova condensates with different chemical and isotopic compositions by their grain sizes, D. D. CLAYTON (1980, 1981b) proposed that Allende inclusion C1, which has a deficit in ^{50}Ti, was formed by aggregation of larger-than-average supernova condensates which were quite refractory and enriched in material from the outer portions of supernova ejecta. He proposed that this explanation accounted for the deficit in ^{48}Ca, ^{50}Ti and cerium and that the light isotopes of magnesium, silicon and calcium in C1 had been lost by sputtering in the interstellar medium. BB-5, which has a much larger negative ^{50}Ti anomaly, should be much more depleted in cerium and the light isotopes of magnesium and calcium. In fact, it has no cerium anomaly and is depleted in the heavy isotopes of magnesium and calcium. Although different nucleosynthetic components certainly have different chemical properties, it is not clear that these have any direct relationship with the chemical properties of the refractory inclusions. Although many of the isotopic anomalies found are characteristic of nucleosynthesis in supernovae, we have yet to recognize the distinctive chemical signatures of the carriers of these anomalies.

A reasonable explanation of the lack of correlation is that reservoirs with distinctive chemical compositions, nuclear anomalies and mass fractionations were formed prior to the condensation of the inclusions now observed, possibly by multiple evaporation-condensation cycles. Such cycles are to be expected in the turbulent protoplanetary accretion disk model of MORFILL (1983) and MORFILL and R. N. CLAYTON (1986a,b). This model envisages turbulent cycling of material through the hotter inner part of the accretion disk; the cycles are sufficiently short (of the order of years) and few in number ($\leq$10) to permit survival of original isotopic and chemical inhomogeneities. Recent models of solar nebula formation have suggested that turbulence may not be as important as previously thought (BOSS, 1988). A recent three-dimensional model of solar system formation shows the development of nonaxisymmetric mass and temperature distributions, with bars of >1500 K extending out to at least 3 A. U. (BOSS, 1988). This model might allow grains to experience several evaporation-condensation cycles at a fixed distance from the sun. Since hibonite is the most refractory mineral commonly found in refractory inclusions it is the most likely to preserve chemical and isotopic anomalies.

Acknowledgements—We thank I. D. Hutcheon for the use of unpublished ion microprobe analyses of BB-6 and A. J. Fahey and E. Zinner for the use of unpublished ion microprobe analyses of DH-H1. We are grateful for valuable discussions with M. Boily, R. N. Clayton, V. Ekambaram and A. Hashimoto. This paper was considerably improved due to the thorough, constructive reviews of E. K. Zinner, G. J. MacPherson and an anonymous reviewer. This work was supported by funds from the National Aeronautics and Space Administration through grants NAG 9-51 (to R. N. Clayton), NAG 9-111 (to A.M.D.) and NAG 9-54 (to L.G.).

Editorial handling: H. Palme

REFERENCES

ALLEN J. M., GROSSMAN L., LEE T. and WASSERBURG G. J. (1980) Mineralogy and petrography of HAL, an isotopically-unusual Allende inclusion. *Geochim. Cosmochim. Acta* **44**, 685–699.

ANDERS E. and EBIHARA M. (1982) Solar system abundances of the elements. *Geochim. Cosmochim. Acta* **46**, 2363–2380.

BAR-MATTHEWS M., HUTCHEON I. D., MACPHERSON G. J. and GROSSMAN L. (1982) A corundum-rich inclusion in the Murchison carbonaceous chondrite. *Geochim. Cosmochim. Acta* **46**, 31–41.

BISCHOFF A. and KEIL K. (1984) Al-rich objects in ordinary chondrites: related origin of carbonaceous and ordinary chondrites and their constituents. *Geochim. Cosmochim. Acta* **48**, 693–709.

BOSS A. P. (1988) Angular momentum transport by gravitational torques in the early solar nebula (abstr.). *Lunar Planet. Sci. XIX*, 122–123.

BOYNTON W. V. (1975) Fractionation in the solar nebula: Condensation of yttrium and the rare earth elements. *Geochim. Cosmochim. Acta* **39**, 569–584.

BOYNTON W. V. and CUNNINGHAM C. C. (1981) Condensation of refractory lithophile trace elements in the solar nebula and in supernovae (abstr.). *Lunar Planet. Sci. XII*, 106–108.

CAMERON A. G. W. (1984) Star formation and extinct radioactivities. *Icarus* **60**, 416–427.

CAMERON A. G. W. and TRURAN J. W. (1977) The supernova trigger for the formation of the solar system. *Icarus* **30**, 447–461.

CLAYTON D. D. (1978) Precondensed matter: key to the early solar system. *Moon and Planets* **19**, 109–137.

CLAYTON D. D. (1980) Chemical and isotopic fractionation by grain size separates. *Earth Planet. Sci. Lett.* **47**, 199–210.

CLAYTON D. D. (1981a) Some key issues in isotopic anomalies: Astrophysical history and aggregation. *Proc. Lunar Planet. Sci. Conf. 12th*, 1781–1802.

CLAYTON D. D. (1981b) Ubiquitous titanium isotope anomalies (abstr.). *Lunar Planet. Sci. XII*, 151–153.

CLAYTON D. D. (1987) Cosmic chemical memory of ^{48}Ca/^{50}Ti correlation (abstr.). *Lunar Planet. Sci. XVIII*, 183–184.

CLAYTON D. D. and LEISING M. D. (1987) ^{26}Al in the interstellar medium. *Phys. Reports* **14**, 1–50.

CLAYTON R. N., GROSSMAN L. and MAYEDA T. K. (1973) A component of primitive nuclear composition in carbonaceous meteorites. *Science* **182**, 485–488.

CLAYTON R. N., MACPHERSON G. J., HUTCHEON I. D., DAVIS A. M., GROSSMAN L., MAYEDA T. K., MOLINI-VELSKO C., ALLEN J. M. and EL GORESY A. (1984) Two forsterite-bearing FUN inclusions in the Allende meteorite. *Geochim. Cosmochim. Acta* **48**, 535–548.

CLAYTON R. N., HINTON R. W. and DAVIS A. M. (1988) Isotopic variations in the rock-forming elements in meteorites. *Phil. Trans. Roy. Soc. Lond.* **A325**, 483–501.

DAVIS A. M. (1984) A scandalously refractory inclusion in Ornans (abstr.). *Meteoritics* **19**, 214.

DAVIS A. M. and GROSSMAN L. (1979) Condensation and fractionation of the rare earths in the solar nebula. *Geochim. Cosmochim. Acta* **43**, 1611–1632.

DAVIS A. M. and HINTON R. W. (1985) Trace element abundances in OSCAR, a scandium-rich refractory inclusion from the Ornans meteorite (abstr.). *Meteoritics* **20**, 633–634.

DAVIS A. M. and HINTON R. W. (1986) Magnesium and titanium isotopic compositions and trace element chemistry of refractory inclusions in the Ornans carbonaceous chondrite (abstr.). *Lunar Planet. Sci. XVII*, 154–155.

DAVIS A. M., TANAKA T., GROSSMAN L., LEE T. and WASSERBURG G. J. (1982) Chemical composition of HAL, an isotopically-unusual Allende inclusion. *Geochim. Cosmochim. Acta* **46**, 1627–1651.

DAVIS A. M., MACPHERSON G. J. and HINTON R. W. (1986) Rims revealed—ion microprobe analysis of individual rim layers in a Vigarano Type A inclusion (abstr.). *Meteoritics* **21**, 349–351.

DEARBORN D. S. P. and BLAKE J. B. (1984) On the composition of the stellar winds of the most massive stars. *Astrophys. J.* **277**, 783–790.

DEARBORN D. S. P. and BLAKE J. B. (1985) On the source of the ^{26}Al observed in the interstellar medium. *Astrophys. J. Lett.* **288**, L21–L24.

DRAKE M. J. and BOYNTON W. V. (1988) Partitioning of rare earth elements between hibonite and melt and implications for nebular condensation of the rare earth elements. *Meteoritics* **23**, 75–80.

EKAMBARAM V., KAWABE I., TANAKA T., DAVIS A. M. and GROSS-

MAN L. (1984) Chemical compositions of refractory inclusions in the Murchison C2 chondrite. *Geochim. Cosmochim. Acta* **48**, 2089–2105.

EKAMBARAM V., KAWABE I., TANAKA T., DAVIS A. M. and GROSSMAN L. (1985) Erratum to "Chemical compositions of refractory inclusions in the Murchison C2 chondrite." *Geochim. Cosmochim. Acta* **49**, 1293.

FAHEY A. and ZINNER E. (1987) Determination of the Fe isotopic ratios in terrestrial minerals and a Lancé hibonite-hercynite inclusion (abstr.). *Lunar Planet. Sci. XVIII*, 277–278.

FAHEY A., GOSWAMI J. N., MCKEEGAN K. D. and ZINNER E. (1985a) Evidence for extreme ^{50}Ti enrichments in primitive meteorites. *Astrophys. J. Lett.* **296**, L17–L20.

FAHEY A. J., GOSWAMI J. N., MCKEEGAN K. D. and ZINNER E. (1985b) Ion probe and track studies of CM hibonites: ^{26}Al, ^{244}Pu and REE (abstr.). *Lunar Planet. Sci. XVI*, 227–228.

FAHEY A. J., GOSWAMI J. N., MCKEEGAN K. D. and ZINNER E. (1985c) Ion probe measurements reveal large Ti isotopic effects in CM hibonites (abstr.). *Lunar Planet. Sci. XVI*, 229–230.

FAHEY A., ZINNER E., CROZAZ G., KORNACKI A. S. and ULYANOV A. A. (1985d) REE and isotopic studies of a coarse-grained CAI from Efremovka (abstr.). *Meteoritics* **20**, 643–644.

FAHEY A., GOSWAMI J. N., MCKEEGAN K. D. and ZINNER E. (1986a) Ti and Mg isotopic measurements in CM and CV meteorites (abstr.). *Lunar Planet. Sci. XVII*, 216–217.

FAHEY A., ZINNER E. and KURAT G. (1986b) Anomalous Ca and Ti in a hercynite-hibonite inclusion from Lance (abstr.). *Meteoritics* **21**, 359–361.

FAHEY A., GOSWAMI J. N., MCKEEGAN K. D. and ZINNER E. (1987a) ^{26}Al, ^{244}Pu, ^{50}Ti, REE, and trace element abundances in hibonite grains from CM and CV meteorites. *Geochim. Cosmochim. Acta* **51**, 329–350.

FAHEY A., GOSWAMI J. N., MCKEEGAN K. D. and ZINNER E. (1987b) More isotopic measurements in CM hibonites: carbon, oxygen and silicon. *Lunar Planet. Sci. XVIII*, 279–280.

FAHEY A. J., GOSWAMI J. N., MCKEEGAN K. D. and ZINNER E. K. (1987c) ^{16}O excesses in Murchison and Murray hibonites: A case against a late supernova injection origin of isotopic anomalies in O, Mg, Ca and Ti. *Astrophys. J. Lett.* **323**, L91–L95.

FEGLEY B. JR. (1986) A comparison of REE and refractory metal oxidation state indicators for the solar nebula (abstr.). *Lunar Planet. Sci. XVII*, 220–221.

GRAY C. M. and COMPSTON W. (1974) Excess ^{26}Mg in the Allende meteorite. *Nature* **251**, 495–497.

GROSSMAN L. and GANAPATHY R. (1976a) Trace elements in the Allende meteorite—I. Coarse-grained, Ca-rich inclusions. *Geochim. Cosmochim. Acta* **40**, 331–344.

GROSSMAN L. and GANAPATHY R. (1976b) Trace elements in the Allende meteorite—II. Fine-grained, Ca-rich inclusions. *Geochim. Cosmochim. Acta* **40**, 967–977.

HARTMANN D., WOOSLEY S. E. and EL EID M. F. (1985) Nucleosynthesis in neutron-rich supernova ejecta. *Astrophys. J.* **217**, 837–845.

HASHIMOTO A., HINTON R. W., DAVIS A. M., GROSSMAN L., MAYEDA T. K. and CLAYTON R. N. (1986) A hibonite-rich Murchison inclusion with anomalous oxygen isotopic composition (abstr.). *Lunar Planet. Sci. XVII*, 317–318.

HINTON R. W. and BISCHOFF A. (1984) Ion microprobe magnesium isotope analysis of plagioclase and hibonite from ordinary chondrites. *Nature* **308**, 169–172.

HINTON R. W. and DAVIS A. M. (1986a) Partitioning of the rare earth elements among the phases of a coarse-grained Allende inclusion (abstr.). *Meteoritics* **20**, 397–398.

HINTON R. W. and DAVIS A. M. (1986b) Trace elements and calcium isotopes in the Murchison corundum-hibonite inclusion GR-1 (abstr.). *Lunar Planet. Sci. XVII*, 344–345.

HINTON R. W., GROSSMAN L. and MACPHERSON G. J. (1984a) Magnesium and calcium isotopes in hibonite-bearing CAIs (abstr.). *Meteoritics* **19**, 240–241.

HINTON R. W., SCATENA-WACHEL D. E. and DAVIS A. M. (1984b) A search for ^{60}Fe in meteorites using the ion probe microanalyser (abstr.). *Lunar Planet. Sci. XV*, 365–366.

HINTON R. W., DAVIS A. M. and SCATENA-WACHEL D. E. (1985a) A large negative titanium-50 anomaly in a refractory inclusion from the Murchison meteorite (abstr.). *Meteoritics* **20**, 664–665.

HINTON R. W., DAVIS A. M. and SCATENA-WACHEL D. E. (1985b) Ion microprobe determination of REE and other trace elements in meteoritic hibonite (abstr.). *Lunar Planet. Sci. XVI*, 352–353.

HINTON R. W., DAVIS A. M. and SCATENA-WACHEL D. E. (1985c) Ion microprobe measurement of calcium and magnesium isotopic mass fractionation in refractory inclusions (abstr.). *Lunar Planet. Sci. XVI*, 354–355.

HINTON R. W., CLAYTON R. N., OLSEN E. J. and DAVIS A. M. (1987a) Isotopic mass fractionation of potassium in the earth compared to the bulk solar system (abstr.). *Lunar Planet. Sci. XVIII*, 429–430.

HINTON R. W., DAVIS A. M. and SCATENA-WACHEL D. E. (1987b) Large negative ^{50}Ti anomalies in refractory inclusions from the Murchison carbonaceous chondrite—evidence for incomplete mixing of neutron-rich supernova ejecta into the solar system. *Astrophys. J.* **313**, 420–428.

HUTCHEON I. D. and NEWTON R. C. (1981) Magnesium isotopes, mineralogy, and mode of formation of secondary phases in C3 refractory inclusions (abstr.). *Lunar Planet. Sci. XII*, 491–493.

HUTCHEON I. D., BAR-MATTHEWS M., TANAKA T., MACPHERSON G. J., GROSSMAN L., KAWABE I. and OLSEN E. (1980) A Mg isotope study of hibonite-bearing Murchison inclusions (abstr.). *Meteoritics* **15**, 306–307.

HUTCHEON I. D., STEELE I. M., WACHEL D. E. S., MACDOUGALL J. D. and PHINNEY D. (1983) Extreme Mg fractionation and evidence of Ti isotopic variations in Murchison refractory inclusions (abstr.). *Lunar Planet. Sci. XIV*, 339–340.

HUTCHEON I. D., ARMSTRONG J. T. and WASSERBURG G. J. (1984) Excess ^{41}K in Allende CAI: confirmation of a hint (abstr.). *Lunar Planet. Sci. XV*, 387–388.

HUTCHEON I. D., ARMSTRONG J. T. and WASSERBURG G. J. (1985) Isotopic studies of Mg, Ca, Fe, Mo and Ru in Fremdlinge (abstr.). *Lunar Planet. Sci. XVI*, 384–385.

HUTCHEON I. D., ARMSTRONG J. T. and WASSERBURG G. J. (1987) Isotopic studies of Mg, Fe, Mo, Ru and W in Fremdlinge from Allende refractory inclusions. *Geochim. Cosmochim. Acta* **51**, 3175–3192.

IRELAND T. R. (1987a) Correlated morphological, chemical, and isotopic systematics from Murchison (C2M) hibonites (abstr.). *Lunar Planet. Sci. XVIII*, 451–452.

IRELAND T. R. (1987b) Correlated morphological, chemical, and isotopic systematics from Murchison (C2M) hibonites (abstr.). *Meteoritics* **22**, 416–417.

IRELAND T. R., COMPSTON W. and HEYDEGGER H. R. (1985) Titanium isotopic anomalies in hibonites from the Murchison carbonaceous chondrite. *Geochim. Cosmochim. Acta* **49**, 1989–1993.

IRELAND T. R., COMPSTON W. and WILLIAMS I. S. (1986) U-Pb age determinations of meteoritic perovskites (abstr.). *Terra Cognita* **6**, 174.

IRELAND T. R., FAHEY A. J. and ZINNER E. K. (1988) Calcium and titanium isotopic systematics of hibonites (abstr.). *Lunar Planet. Sci. XIX*, 527–528.

IRVING A. J. (1978) A review of experimental studies on crystal/liquid trace element partitioning. *Geochim. Cosmochim. Acta* **42**, 743–771.

LATTIMER J. M., SCHRAMM D. N. and GROSSMAN L. (1977) Supernovae, grains and the formation of the solar system. *Nature* **269**, 116–118.

LAUGHLIN J. R., HINTON R. W., DAVIS A. M. and GROSSMAN L. (1986) Ion microprobe study of rim and core perovskite in an Allende inclusion (abstr.). *Meteoritics* **21**, 430–431.

LEE T., PAPANASTASSIOU D. A. and WASSERBURG G. J. (1976) Demonstration of ^{26}Mg excess in Allende and evidence for ^{26}Al. *Geophys. Res. Lett.* **3**, 109–112.

LEE T., RUSSELL W. A. and WASSERBURG G. J. (1979) Calcium isotopic anomalies and the lack of aluminum-26 in an unusual Allende inclusion. *Astrophys. J. Lett.* **228**, L93–L98.

LEE T., MAYEDA T. K. and CLAYTON R. N. (1980) Oxygen isotopic anomalies in Allende inclusion HAL. *Geophys. Res. Lett.* **7**, 493–496.

LONG J. V. P. and HINTON R. W. (1984) The intensity of metal

hydride peaks in secondary positive-ion spectra from silicates. *Intl. J. Mass Spectrom. Ion Processes* **55**, 307–318.

MACPHERSON G. J., BAR-MATTHEWS M., TANAKA T., OLSEN E. and GROSSMAN L. (1983) Refractory inclusions in the Murchison meteorite. *Geochim. Cosmochim. Acta* **47**, 823–839.

MACPHERSON G. J., GROSSMAN L., HASHIMOTO A., BAR-MATTHEWS M. and TANAKA T. (1984) Petrographic studies of refractory inclusions from the Murchison meteorite. *Proc. Lunar Planet. Sci. Conf. 15th*, C299–C312.

MACPHERSON G. J., GROSSMAN L., HASHIMOTO A., BAR-MATTHEWS M. and TANAKA T. (1985) Correction to "Petrographic studies of refractory inclusions from the Murchison meteorite". *Proc. Lunar Planet. Sci. Conf. 15th*, C843.

MACPHERSON G. J., HINTON R. W. and DAVIS A. M. (1986) Petrology, chemistry and magnesium isotope systematics of a unique Allende inclusion (abstr.). *Meteoritics* **21**, 439–440.

MARTIN P. M. and MASON B. (1974) Major and trace elements in the Allende meteorite. *Nature* **249**, 333–334.

MASON B. and MARTIN P. M. (1977) Geochemical differences among components of the Allende meteorite. *Smithson. Contrib. Earth Sci.* **19**, 84–95.

MORFILL G. E. (1983) Some cosmochemical consequences of a turbulent protoplanetary cloud. *Icarus* **53**, 41–54.

MORFILL G. E. and CLAYTON R. N. (1986a) Oxygen isotope fractionation in the primitive solar nebula: bulk properties (abstr.). *Lunar Planet. Sci. XVII*, 567–568.

MORFILL G. E. and CLAYTON R. N. (1986b) Oxygen isotope fractionation in the primitive solar nebula: theory (abstr.). *Lunar Planet. Sci. XVII*, 569–570.

MYSEN B. O. and VIRGO D. (1980) Trace element partitioning and melt structure: an experimental study at 1 atm pressure. *Geochim. Cosmochim. Acta* **44**, 1917–1930.

NAGASAWA H., SCHREIBER H. D. and MORRIS R. V. (1980) Experimental mineral/liquid partition coefficients of the rare earth elements (REE), Sc and Sr for perovskite, spinel and melilite. *Earth Planet. Sci. Lett.* **46**, 431–437.

NIEDERER F. R. and PAPANASTASSIOU D. A. (1984) Ca isotopes in refractory inclusions. *Geochim. Cosmochim. Acta* **48**, 1279–1293.

NIEDERER F. R., PAPANASTASSIOU D. A. and WASSERBURG G. J. (1985) Absolute isotopic abundances of Ti in meteorites. *Geochim. Cosmochim. Acta* **49**, 835–851.

PAPANASTASSIOU D. A. (1986) Chromium isotopic anomalies in the Allende meteorite. *Astrophys. J. Lett.* **308**, L27–L30.

PEDLEY J. B. and MARSHALL E. M. (1983) Thermochemical data for gaseous monoxides. *J. Phys. Chem. Ref. Data* **12**, 967–1031.

REED S. J. B. (1981) Secondary ion spectra of rare earths. In *Microbeam Analysis—1981* (ed. R. H. GEISS), pp. 87–90. San Francisco Press.

REED S. J. B. (1983) Secondary-ion yields of rare earths. *Intl. J. Mass Spectrom. Ion Processes* **54**, 31–40.

REED S. J. B. (1986) Ion microprobe determination of rare earth elements in accessory minerals. *Mineral. Mag.* **50**, 3–15.

SCATENA-WACHEL D. E., HINTON R. W. and DAVIS A. M. (1984) Preliminary ion microprobe study of chromium isotopes in Orgueil (abstr.). *Lunar Planet. Sci. XV*, 718–719.

SCATENA-WACHEL D. E., HINTON R. W. and DAVIS A. M. (1985) A search for extinct ^{53}Mn and ^{60}Fe in meteorites (abstr.). *Meteoritics* **20**, 751–752.

SCATENA-WACHEL D. E., JONES A. P., MARIANO A., HINTON R. W. and CLAYTON R. N. (1986) Strontium isotopes of kimberlites and carbonatites (abstr.). *Terra Cognita* **6**, 202.

STALEY H. G. and NORMAN J. M. (1969) Thermodynamics of gaseous monoxide-dioxide equilibria for cerium, praseodymium and neodymium. *Int. J. Mass Spectrom. Ion Phys.* **2**, 35–43.

STEELE I. M., HUTCHEON I. D., SOLBERG T. N., SMITH J. V. and CLAYTON R. N. (1977) Effects of energy selection on quantitative analysis in secondary ion microanalysis. *Intl. J. Mass Spectrom. Ion Phys.* **23**, 293–305.

STORMS H. A., BROWN K. F. and STEIN J. D. (1977) Evaluation of a cesium positive ion source for secondary ion mass spectrometry. *Analyt. Chem.* **49**, 2023–2030.

ZINNER E. and CROZAZ G. (1986) A method for the quantitative measurement of rare earth elements in the ion microprobe. *Intl. J. Mass Spectrom. Ion Processes* **69**, 17–38.

ZINNER E. and EPSTEIN S. (1987) Heavy carbon in individual oxide grains from the Murchison meteorite. *Earth Planet. Sci. Lett.* **84**, 359–368.

ZINNER E., FAHEY A., GOSWAMI J., IRELAND T. and MCKEEGAN K. (1986) Large ^{48}Ca anomalies are associated with ^{50}Ti anomalies in Murchison and Murray hibonites. *Astrophys. J. Lett.* **311**, L103–L107.

ZINNER E., FAHEY A., GOSWAMI J. and MCKEEGAN K. (1987) Isotopic structures in Murchison hibonites: O, Ca, and Ti (abstr.). *Meteoritics* **22**, 542–543.

6. APPENDIX

6.1 Calcium and magnesium mass fractionation

Nuclear isotope anomalies in calcium are principally confined to ^{48}Ca; while anomalies are seen at other masses, these are generally small compared to mass fractionation effects (NIEDERER and PAPANASTASSIOU, 1984). Measurement of calcium isotopes on our ion microprobe is effectively limited to ^{40}Ca, ^{42}Ca, ^{43}Ca and ^{44}Ca, since ^{46}Ca and ^{48}Ca are overlapped by ^{46}Ti and ^{48}Ti, respectively. The large ^{48}Ti/^{48}Ca ratio observed in hibonite and the incomplete separation of $^{48}Ca^+$ from $^{48}Ti^+$ at the maximum mass resolution of the Chicago ion microprobe ($M/\Delta M = 5000$) makes high precision measurement of ^{48}Ca/^{40}Ca ratios virtually impossible. Measurement of calcium mass fractionation using $^{40}Ca^+$, $^{42}Ca^+$ and $^{44}Ca^+$ is difficult, because of isobaric interferences from molecular ions such as MgO^+ and SiO^+. We have found that there is a significant yield of Ca^{2+} ions and that the yields of MgO^{2+} and SiO^{2+} are very low. Measurement of calcium mass fractionation can readily be made at low mass resolution by measuring Ca^{2+} at $m/e = 20$, 21 and 22. The ion yield of Ti^{2+} is also much lower than that of Ca^{2+}, but $^{48}Ca^{2+}$ cannot be measured because of interference from $^{24}Mg^+$. The proportion of singly charged to doubly charged calcium ions varies from matrix to matrix. In hibonite, the Ca^+/Ca^{2+} ion yield ratio is approximately 100 while pyroxene, apatite and calcite have Ca^+/Ca^{2+} ratios of 40, 300 and 10^4, respectively.

Calcium mass fractionation was determined by making alternate short runs (20 sweeps through m/e = 20, 21 and 22 in 10 minutes) on unknowns and terrestrial standards of similar chemical composition. Terrestrial standards used were Madagascar hibonite, a natural diopside and synthetic anorthite glass. Under normal operating conditions, observed variations in the ^{44}Ca/^{40}Ca ratio calculated in the standard from one run to the next were less than $\pm 2\%$ (2σ).

In our initial analyses (HINTON *et al.*, 1985c), each sample lay within statistical uncertainty but slightly to the ^{42}Ca-rich side of the terrestrial mass fractionation line. Mg^+ scattering was initially ruled out (HINTON *et al.*, 1985c) since other low-magnesium hibonite, such as HAL, seemed to show the same effect. Subsequent analyses have shown that only the Madagascar hibonite standard, with at least three times more magnesium than the unknowns, has a significant deviation from the terrestrial fractionation line, having an excess of ~ 3‰ at $m/e = 21$ not attributable to $^{42}Ca^{2+}$. The excess at $m/e = 21$ is probably due to a $^{25}Mg^+$ scatter peak which has been observed in magnesium-rich minerals such as olivine. The scatter peak is believed to be due to Mg^+ ions striking some portion of the mass spectrometer and may be very sensitive to tuning conditions. Since it is difficult to be certain that the correction would remain constant for all tuning conditions used, $^{42}Ca^{2+}$ was not used for calculating calcium isotopic mass fractionation in hibonite. The largest effect that the Mg^+ scatter peak could have on Δ^{44}Ca is ≤ 0.2‰/amu.

Low mass resolution analyses of calcium isotope fractionation can be extended to calcic pyroxene and plagioclase, both of which have significant Ca^{2+} yields. Precisions of ± 1.0‰/amu can readily be obtained for these two phases. Values measured in pyroxene and plagioclase do not depart significantly from a linear fractionation line passing through normal calcium on a ^{44}Ca/^{40}Ca *vs.* ^{42}Ca/^{40}Ca plot, presumably because the intensity of Mg^+ scatter peaks is lower. Analyses of fassaite in several of the EGG series coarse-grained Allende inclusions show excellent agreement with the data obtained by thermal ionization mass spectrometry with a double isotopic spike (NIEDERER and PAPANASTASSIOU, 1984), Table A1. EGG-1 and EGG-2 give normal values for ΔCa; EGG-3 gives the expected value of ~ -1‰/amu; and EGG-6, not analyzed by NIEDERER and PAPANASTASSIOU (1984), shows ΔCa value of $-1.6 \pm .8$‰/amu. Calcium

Table A1. Calcium isotopic mass fractionation of CAI pyroxene, relative to terrestrial diopside and of terrestrial plagioclase, relative to anorthite glass. Uncertainties are ±2σ.

Sample	$\Delta^{42}Ca$* (‰/amu)	$\Delta^{44}Ca$† (‰/amu)	ΔCa_M‡ (‰/amu)	$\Delta^{44}Ca$§ (‰/amu)
EGG-1	+2.5 ± 4.1	0.0 ± 1.6	+0.3 ± 1.5	+0.1
EGG-2	-0.8 ± 1.5	-0.9 ± 0.8	-0.9 ± 0.7	-0.2
EGG-3	-1.4 ± 1.1	-1.2 ± 0.9	-1.3 ± 0.7	-1.0
EGG-6	-0.7 ± 2.0	-1.8 ± 0.9	-1.6 ± 0.8	—
An_{80}	-0.6 ± 2.8	+0.3 ± 1.4	+0.1 ± 1.3	—
An_{69}	+1.0 ± 1.9	-1.1 ± 0.8	-0.8 ± 0.7	—
An_{60}	-0.2 ± 2.9	+0.8 ± 1.0	+0.7 ± 1.0	—
Mean Plagioclase	—	—	-0.2 ± 0.5	—

$$*\Delta^{42}Ca = \frac{(^{42}Ca/^{40}Ca)_{unknown} - (^{42}Ca/^{40}Ca)_{standard}}{(^{42}Ca/^{40}Ca)_{standard}} \times \frac{1000}{2}.$$

$$\dagger\Delta^{44}Ca = \frac{(^{44}Ca/^{40}Ca)_{unknown} - (^{44}Ca/^{40}Ca)_{standard}}{(^{44}Ca/^{40}Ca)_{standard}} \times \frac{1000}{4}.$$

‡ΔCa_M = mean of $\Delta^{42}Ca$ and $\Delta^{44}Ca$, weighted by uncertainties.

§values of NIEDERER and PAPANASTASSIOU (1984), by thermal ionization mass spectrometry with double isotopic spike, equal to -Δ40 in their notation .

isotopic analyses of feldspar glasses show no variation in mass fractionation with chemical composition (Table A1).

The procedures used for measurement of magnesium isotopic compositions, both for mass fractionation and for nuclear anomalies at ^{26}Mg, have been given by R. N. CLAYTON *et al.* (1984). Mg^+ and Ca^{2+} require different electron multiplier settings, so they were not measured at the same time. Calcium and magnesium mass fractionation determinations were only made when a number of repeat measurements could be made on the same sample. These measurements were not made on MUCH-1 and BB-6, because it was difficult to repeatedly place the ion microprobe primary beam spot on hibonite free of surrounding matrix.

6.2 *Barium and rare earth elements*

Barium and REE were determined at low mass resolution by computer-controlled magnetic peak switching. Intensities at every *m/e* value from 192 (194 in later runs) to 135 were recorded for 10 seconds each per scan. At least 7 scans were made for each REE analysis and 60 were made of the HAL hibonite standard. Background count rates for this instrument are typically one count per minute; this is approximately equivalent to 9 ppb La for a 5 nA primary beam under energy filtering conditions.

In order to obtain concentrations from these count rates, it is necessary to know ion yields and to correct for molecular interferences. Relative ion yields in a given matrix are quite constant, but absolute ion yields can vary from day to day because of differences in primary ion bombardment conditions and secondary ion extraction tuning. For this reason, ratios of count rates were measured and normalized to a single element. Calcium was used as a reference element in hibonite because it is quite constant in concentration. Its concentration was calculated from $CaAl_{12}O_{19}$ stoichiometry assuming substitution of minor and trace elements for aluminum only.

In brief, count rates were collected in the REE mass range, corrected for molecular interferences and converted to relative concentrations using ion yields. Absolute concentrations were determined from separate measurements of relative count rates of cerium and calcium.

6.2.1 Suppression of molecular interferences. Determination of relative concentrations for both LREE and HREE requires elimination of molecular interferences from the hibonite matrix and correction for monoxide ions of barium and LREE. On a plot of ion yield *vs.* secondary ion energy, ion yields of all species have maxima at about the same ion energy, but the energy distributions of molecular ions are narrower than those of monatomic ions, so molecular interferences can be reduced by making measurements at high ion energies. Further, molecular ions containing many atoms have narrower energy distributions than those with fewer atoms. Long chain molecules are therefore easier to discriminate against than less complex molecules such as LnO^+ and $LnAl^+$.

Hibonite is a simple substrate containing low concentrations of elements with $Z > 56$. Molecular ions with *m/e* between 135 and 192 (except combinations of REE and major elements) must therefore consist of three or more atoms. When the ion microprobe is tuned for maximum intensity the most intense molecular ion with more than two atoms in the Ln^+ *m/e* range is $CaAl_2O_3^+$ at *m/e* = 142. This species can be shown to be significantly reduced by the use of energy filtering. Energy filtering on the Chicago ion microprobe is accomplished by increasing the voltage on the repeller, a small bent wire very close to the beam spot. The energy of ions transmitted through the secondary ion optics of the ion microprobe increases with increasing repeller voltage (STEELE *et al.*, 1977). A plot of Ca^+, Ce^+, CeO^+ and $CaAl_2O_3^+$ against repeller voltage is given in Fig. A1. $CaAl_2O_3^+$ is reduced by at least a factor of 10^3 and CeO^+ is reduced by a factor of 30–40 when Ce^+ is reduced by a factor of only 10. While neither the absolute energy nor the energy window can be defined for the Chicago ion microprobe, ion yield *vs.* repeller voltage profiles for Ln^+ and LnO^+ can be compared with ion yield *vs.* secondary ion energy profiles measured on a Cameca IMS 3F ion microprobe (REED, 1983). The degree of LnO^+ suppression indicates that the hibonite data reported in this study were measured at an energy of ≤30 eV. $LnAl^+$ and LnO_2^+ are molecular species not completely eliminated here by energy filtering. LnO_2^+ and $LnAl^+$ ions (principally those of lanthanum, cerium and praseodymium) were observed in the mass spectrum of Madagascar hibonite because of its very high LREE/HREE ratio. While LaO_2^+ and CeO_2^+ are considerably reduced by energy filtering, $CeAl^+$ actually increases relative to Ce^+. The measured $CeAl^+/Ce^+$ ratio increased from 0.00064 to 0.0010 in going from normal to energy-filtering conditions, thus vi-

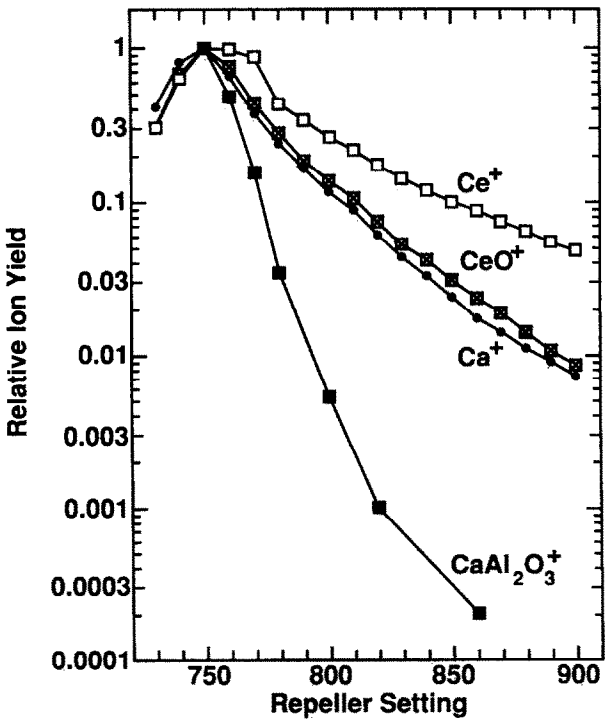

FIG. A1. Secondary ion intensities of $^{40}Ca^+$, $^{140}Ce^+$, $^{140}Ce^{16}O^+$ and $^{40}Ca^{27}Al_2^{16}O_3^+$ (all normalized to 1 at a repeller setting of 750) *vs.* repeller setting. The repeller setting is proportional to ion energy.

olating the general rule that molecular species have narrower energy distributions than single ions. Measured LnO_2^+/Ln^+ ratios for lanthanum, cerium and praseodymium in Madagascar hibonite are ~0.00019, ~0.00060 and ~0.00016, respectively, under energy-filtering conditions. Corrections were made to all runs using these values. In meteoritic samples calculated REE abundances are not significantly different if no correction is applied, because meteoritic hibonite always has lower LREE/HREE ratios than Madagascar hibonite. LnO_2^+ represents less than 10 ppb Yb when the LREE concentrations are 50 times C1 chondritic.

Energy filtering is assumed to remove all molecular species except LnO^+, BaO^+, LnO_2^+ and $LnAl^+$ at the masses used in the deconvolution procedure. La^+ could not be used to set the degree of energy filtering because interferences at m/e = 139 occur under unfiltered conditions. Ca^+ could not be used as it has a much narrower energy distribution than Ln^+; its energy distribution is very similar to that of CeO^+ (Fig. A1). The level of energy filtering was set by reducing the $^{48}Ti^+$ intensity by exactly 10 times compared to unfiltered conditions. Titanium is present in reasonable abundance in all hibonite and Ti^+ has an energy distribution similar to that of Ln^+.

6.2.2 Monoxide deconvolution procedure. Correction for the LREE LnO^+ interference at the m/e values of HREE can be achieved through use of simultaneous equations; however, low count rates encountered in some samples cause statistical uncertainties to be propagated unfavorably when this procedure is employed. Further, strong similarity between the GdO^+ and Yb^+ isotopic abundance pattern and the overlap of monoisotopic $^{159}Tb^{16}O^+$ on $^{175}Lu^+$, the only major isotope of lutetium, prevents use of simultaneous equations in these two cases. LnO^+ peaks of HREE cannot be used to measure concentrations, as in REED (1981), because m/e values above 176 may have contributions from other elements, most notably hafnium and the platinum metals. HREE can be determined by oxide deconvolution if the relationships of LREE LnO^+/Ln^+ ratios to one another are known under varying recording and matrix conditions. In order to determine these relationships, measurements were made of LnO^+/Ln^+ ratios for lanthanum, cerium, praseodymium, neodymium and samarium in Madagascar hibonite under varying degrees of energy filtering. HREE are significantly depleted in this sample and LnO^+ species of LREE dominate the Ln^+ m/e values of HREE even under the most extreme energy filtering conditions used. The amount of energy filtering used was limited by the requirement of detecting a useful ion signal. A plot of LnO^+/Ln^+ *vs.* NdO^+/Nd^+ shows that LnO^+/Ln^+ ratios remain in constant proportion to one another regardless of the degree of energy filtering (Fig. A2). The LnO^+/Ln^+ ratios are assumed to behave similarly for barium, europium, gadolinium and terbium. The relationship between LnO^+/Ln^+ ratios for the various REE agree reasonably well with the values obtained for calcium aluminum silicate glasses by REED (1983). The LnO^+/Ln^+ ratios for europium, gadolinium and terbium, relative to that of neodymium, have been taken from his work. The value for BaO^+/Ba^+ was taken from that measured relative to LaO^+/La^+ on a Corning borosilicate glass standard.

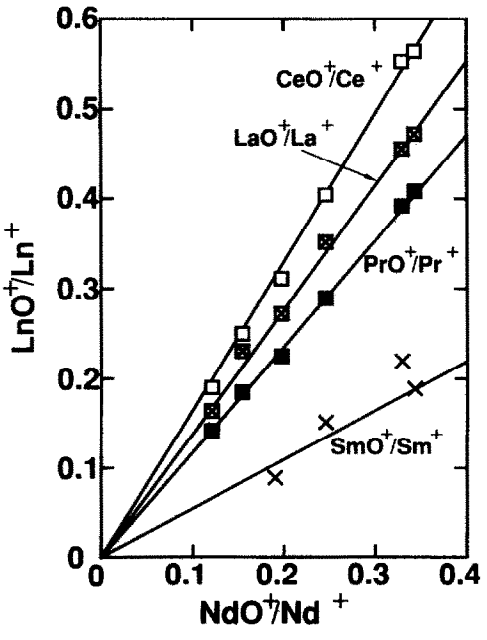

FIG. A2. Element to oxide ion yield ratios for cerium, lanthanum, praseodymium and samarium *vs.* neodymium in Madagascar hibonite. Ratios measured at different ion energies lie along lines of constant slope that pass through the origin.

Table A2. Monoxide/monatomic ion yield ratios and lanthanum-normalized ion yields, measured at high ion energy.

Element	Ion Yield	MO^+/M^+
Ba	1.000	0.052
La	1.000	0.49
Ce	0.863	0.55
Pr	0.961	0.41
Nd	1.059	0.33
Sm	1.196	0.18
Eu	1.471	0.11
Gd	0.941	0.326
Tb	0.941	0.288
Dy to Lu	0.941	—

The deconvolution procedure initially assumes an average set of LnO^+/Ln^+ ratios (Table A2). The procedure first corrects for $^{135,137}Ba^{16}O^+$ overlap on $^{151,153}Eu^+$, then $^{151}Eu^{16}O^+$ on $^{167}Er^+$, $^{168}Er^+$ on $^{152}Sm^{16}O^+$, $^{147}Sm^{16}O^+$ on $^{163}Dy^+$ and finally $^{162}Dy^+$ on $^{146}Nd^{16}O^+$. Once the NdO^+/Nd^+ ratios are determined, this ratio is then used to recalculate the BaO^+/Ba^+, PrO^+/Pr^+, etc. ratios, simply by multiplying the ratios given in Table A2 by $(NdO^+/Nd^+)_{obs.}/(NdO^+/Nd^+)_{Table\ A2}$. This procedure is repeated until the difference in the NdO^+/Nd^+ ratio between iterations is less than 1‰. The deconvolution procedure converges rapidly and only rarely were more than two iterations required. NdO^+/Nd^+ ratios were generally in the range 0.20–0.30. In this procedure, the major interfering species, NdO^+ and SmO^+, are determined separately and the constancy of the $(NdO^+/Nd^+)/(SmO^+/Sm^+)$ ratio is an independent check of the deconvolution procedure. The SmO^+/Sm^+ ratio can also be fixed relative to that of the NdO^+/Nd^+ ratio; the use of this procedure does not significantly change any of the results reported here. Alternatively, since $^{139}La^{16}O^+$ and $^{140}Ce^{16}O^+$ are usually much more intense than $^{155}Gd^+$ and $^{156}Gd^+$, respectively, once an approximate Gd^+ count rate is established using m/e = 157 and 160, the LaO^+/La^+ or CeO^+/Ce^+ ratio can be calculated and could be used to determine the other LnO^+ count rates.

6.2.3 Selection of m/e values for REE determination. The isotopes used to determine LREE concentrations were 139 for lanthanum; 140 for cerium; 141 for praseodymium; 143, 144, 145 and 146 for neodymium; 149 and 152 for samarium; and 151 and 153 for europium. Barium was determined using m/e = 138. M/e = 147 was not used for samarium due to the presence of an unknown interference which could not be reduced by energy filtering. The isotopes used to determine the HREE concentrations were 157 and 160 for gadolinium; 159 for terbium; 161, 162, 163 and 164 for dysprosium; 165 for holmium; 166, 167 and 168 for erbium; 169 for thulium; 171, 172, 173 and 174 for ytterbium; and 175 for lutetium. Gadolinium is determined using only isotopes 157 and 160, because there are large overlaps from LaO^+, CeO^+ and NdO^+ at m/e = 155, 156 and 158.

6.2.4 Determination of ion yields relative to lanthanum. The Ba^+ ion yield was determined on Corning borosilicate glass, relative to La^+ and Ce^+, under both normal and energy filtered conditions. LREE ion yields, relative to that of La^+ (Table A2), have been determined for Nd^+, Sm^+ and Eu^+ using the concentrations given for HAL hibonite (sample 2, free of titanium-rich needles) by RNAA (DAVIS *et al.*, 1982). The ion yield for Ce^+, relative to that of La^+, was deter-

mined from electron microprobe measurements of the La/Ce ratio of Madagascar hibonite (I. D. HUTCHEON, pers. commun.). The Pr^+ ion yield was determined by interpolation between the Ce^+ and Nd^+ ion yields.

Ion yields of the HREE are more difficult to determine because of the low concentrations of these elements in the HAL standard. The most consistent HREE patterns are obtained if the ion yields of the HREE are assumed to be uniform. Admittedly, ion yields which smoothly increase or decrease would also give smooth patterns. HREE ion yields determined by ZINNER and CROZAZ (1986) also suggest that there is little variation in their relative yields (with the possible exceptions of gadolinium and lutetium). The ion yields used here are calculated to give concentrations for HAL hibonite similar to those given by DAVIS *et al.* (1982), weighted towards the more abundant elements.

6.2.5 Determination of absolute concentrations. Ion yields of Ce^+ and La^+, relative to that of Ca^+, were determined under normal extraction conditions using HAL and Madagascar hibonite. The absolute concentrations of cerium (or lanthanum for HAL and DH-H1) were calculated from ion yields so obtained using ion count rates measured on unknowns, without energy filtering applied, at the *m/e* values for ^{140}Ce (or ^{139}La) and ^{44}Ca. La^+ was not routinely used because of the presence of molecular interferences at *m/e* = 139 in hibonite high in magnesium and titanium. The absolute concentrations determined for lanthanum using these yields are in very good agreement with those obtained in the bulk inclusions by neutron activation analysis for BB-5 and MUCH-1 (when normalized to calcium).

Since the LREE concentrations in GR-1 rim hibonite were very low, lanthanum and cerium intensities recorded without energy filtering may be significantly affected by normally minor molecular interferences. Absolute abundances of REE were calculated from the yttrium concentration, assuming that the hibonite had the C1 chondritic Ho/Y ratio of 0.0366. The cerium count rate observed at *m/e* = 140 without energy filtering suggests a concentration 20% higher than the value in Table 2. The REE concentrations in GR-1 rim hibonite reported in HINTON and DAVIS (1986b) were calculated using observed count rates under energy filtering conditions and are approximately 60% lower than those reported here. The absolute abundances in BB-5 and GR-1 corundum and BB-5 HREE-rich phases (BB-5-O, BB-5-A and BB-5-B) were also determined from the yttrium concentration.

6.3 Other minor and trace elements

Trace element determinations were made by measuring intensities from *m/e* = 100 to 20 at low mass resolution without energy filtering. *M/e* = 40 (Ca^+) and 27 (Al^+) were normally excluded to avoid overloading the electron multiplier. All ion yields were normalized to Ca^+ (using $^{44}Ca^+$ intensities); the Ca^+ ion yield was ~25 counts s^{-1} ppm^{-1} nA^{-1}.

Ion yields for Mg^+, Si^+, Ti^+ and Sr^+, relative to Ca^+, were initially calculated using electron microprobe determinations of Madagascar hibonite (I. D. Hutcheon analyses by wavelength dispersion and R. W. Hinton analyses by energy dispersion). Sc^+ ion yields were determined using INAA data for MUCH-1 (EKAMBARAM *et al.*, 1984) assuming that all calcium and scandium in both the INAA and ion microprobe samples is present in hibonite. Ion yields for all other elements were determined using intensities measured on three doped borosilicate glasses made by Corning. Intensities were recorded on these glasses manually, corrected for drift in intensity with time and for molecular interferences. Intensities were then normalized to $^{42}Ca^+$, because of a substantial $^{28}Si^{16}O^+$ interference on $^{44}Ca^+$. Comparison of Ca^+-normalized ion yields for pure metals (STORMS *et al.*, 1977), Corning borosilicate glasses, plagioclase and Madagascar hibonite (Table A3), suggest that ion yields for elements for which no hibonite standard was available are within ~30% of the true value. Ti^+ ion yields appear to be sensitive to the matrix and, in hibonite, appear to vary with titanium content; this is discussed below.

Possible or known interferences at the masses used to determine the trace element concentrations are discussed below. Despite the presence of significant interferences at the ppm level, the uncorrected upper limits are often much lower than those set by electron microprobe and INAA.

6.3.1 $^{23}Na^+$. No major interferences are known. The most likely interference, $^{46}Ti^{2+}$, can be shown to be equivalent to less than 0.1 ppm Na for a sample with 3 wt% Ti by using intensities recorded for $^{49}Ti^{2+}$ at *m/e* = 24.5 to set limits on the Ti^+/Ti^{2+} ratio ($>6 \times 10^3$). Li^+ counts (and therefore the possibility of a $^7Li^{16}O^+$ interference) were observed in one run made on HAL hibonite. No large Li^+ count rate was observed in any of the runs reported here. No corrections were made for molecular species.

6.3.2 $^{24}Mg^+$. Corrections are made for $^{48}Ca^{2+}$, as described by BARMATTHEWS *et al.* (1982). The largest correction for this species was 2% (relative) for magnesium in DH-H1. $^{48}Ti^{2+}$ represents less than 0.7 ppm Mg for every 1 wt% Ti; no corrections were made for this species.

6.3.3 $^{28}Si^+$. $^{27}Al^1H^+$ is a potential interference; fortunately, aluminum does not form a strong hydride ion. The Al^+/AlH^+ ratio is ~7 times greater than the Si^+/SiH^+ ratio (LONG and HINTON, 1984). The limit set by HAL hibonite indicates that the Al^+/AlH^+ ratio is $>7 \times 10^4$ and AlH^+ represents less than 60 ppm Si in hibonite. No correction was made for this species. Elevated Si^+ count rates are usually indicative of overlap of the ion beam onto the surrounding, principally silicate, matrix. Where repeat analyses were made on the same area or grain, those with the lowest apparent silicon content were taken as being most representative of hibonite.

6.3.4 $^{39}K^+$. $^{23}Na^{16}O^+$ is a possible interference; however, the NaO^+/Na^+ ratios measured in An_{60} feldspar demonstrate that this species represents less than 0.1 ppm K for all hibonite analyzed here.

6.3.5 $^{44}Ca^+$. Interferences at *m/e* = 44 include $^{27}Al^{16}O^1H^+$ and $^{28}Si^{16}O^+$. Analyses of BB-5-C indicate that the $AlO^+/AlOH^+$ ratio is greater than 500 and that $AlOH^+$ represents less than 0.2% of the *m/e* = 44 count rate. High resolution measurements give a SiO^+/Si^+ ratio of 0.036; SiO^+ represents less than 1% of the e/e = 44 count rate.

6.3.6 $^{45}Sc^+$. A limit to the intensity of $^{44}Ca^1H^+$ was set in the low potassium and magnesium HAL hibonite by measuring Ca^+ and CaH^+ at *m/e* = 40 and 41. CaH^+ represents less than 0.07 ppm Sc for each 1% Ca. $^{29}Si^{16}O^+$ is more significant: high mass resolution measurements of $^{28}Si^{16}O^+$ at *m/e* = 44 show that SiO^+ is equivalent to ~3 ppm Sc for every 1 wt% Si; this correction is only significant in BB-6 hibonite.

6.3.7 $^{48}Ti^+$. A correction is made for $^{48}Ca^+$ using the $^{44}Ca^+$ intensity. A high resolution study (HINTON *et al.*, 1987b) determined that $^{24}Mg_2^+$ is equivalent to 5 ppm Ti for every 1% Mg. Comparison between Ti^+ count rates and electron microprobe-determined Ti concentrations suggests that its ion yield decreases by approximately 30% when the Ti content increases from 1 to 4%.

6.3.8 $^{51}V^+$. $^{25}Mg^{26}Mg^+$ is equivalent to 0.2 ppm V for every 1% Mg. The $^{24}Mg^{27}Al^+$ contribution can be substantial and often constitutes more than half the intensity recorded at *m/e* = 51. The applied correction determined in section 6.3.9 corresponds to 65 ppm V for every 1 wt% Mg.

Table A3. Calcium-normalized ion yields, measured with no energy filtering applied. Ion yields in boldface were used.

Element	Isotope	Madagascar hibonite	Corning glass	Lake County plagioclase	Pure Metal*
Na	^{23}Na	—	—	**2.46**	—
Mg	^{24}Mg	**0.785**	0.763	0.756	—
Si	^{28}Si	**0.114**	0.175	0.128	0.129
K	^{39}K	—	**1.74**	2.34	—
Ca	^{44}Ca	**1.000**	**1.000**	**1.000**	**1.000**
Sc	^{45}Sc	**0.457**†	—	—	—
Ti	^{48}Ti	**0.278**	0.450	0.342	0.444
V	^{51}V	—	**0.348**	—	0.378
Cr	^{52}Cr	—	**0.325**	—	0.378
Mn	^{55}Mn	—	**0.179**	—	0.153
Sr	^{88}Sr	**0.685**	0.483	0.577	—
Y	^{89}Y	—	**0.216**	—	—
Zr	$^{91,92}Zr$	—	**0.114**	—	0.113
La	^{139}La	**0.188**‡	0.178	—	—
Ce	^{140}Ce	**0.154**‡	0.156	—	—

*STORMS *et al.* (1977). †MUCH-1 (calcium-normalized). ‡HAL and Madagascar hibonites.

6.3.9 $^{52}Cr^+$. Intensities at m/e = 52 and 53 are dominated by Cr^+, $^{25}Mg^{27}Al^+$ and $^{26}Mg^{27}Al^+$; if the $^{26}Mg/^{25}Mg$ ratio is known, intensities of these species can therefore be calculated using simultaneous equations. The calculated $MgAl^+/Mg^+$ ratio (0.0036) was constant to ±5% (2σ) in analyses not limited by counting statistics. This value agrees reasonably well with a measurement of the $MgAl^+$ intensity made at high mass resolution at m/e = 51 in low-vanadium Madagascar hibonite ($MgAl^+/Mg^+$ = 0.0030). Poor counting statistics usually limited the use of simultaneous equations; corrections were made at m/e = 51 and 52 assuming a constant $MgAl^+/Mg^+$ ratio of 0.0036. $MgAl^+$ is equivalent to 9 ppm Cr for every 1 wt% Mg.

6.3.10 $^{55}Mn^+$. $^{27}Al^{28}Si^+$ can be significant if hibonite has a high silicon content or if the primary beam partially overlaps a silicate phase. Samples with low manganese content give an upper limit of 0.0025 to the $AlSi^+/Si^+$ ratio; $AlSi^+$ is therefore equivalent to <15 ppm Mn for every 1 wt% Si. This correction amounts to more than 50% of the m/e = 55 intensity only in GR-1 hibonite.

6.3.11 $^{88}Sr^+$. Ca_2^+ and $CaMgO^+$ are negligible, accounting for <0.06 ppm Sr. $^{45}Sc^{27}Al^{16}O^+$ is more significant. This species cannot, however, be measured directly, even at high mass resolution. Initially, the $ScAlO^+/Sc^+$ ratio was assumed to be the same as that of $CaAlO^+/Ca^+$. Results given for GR-1 in HINTON and DAVIS (1986b) used this correction. Analysis of the mixed phase within BB-5 corundum and scandium-rich phases within the OSCAR inclusion from Ornans (DAVIS, 1984; DAVIS and HINTON, 1985) indicates that the $ScAlO^+/Sc^+$ ratio is approximately 2.7 times lower than the $CaAlO^+/Ca^+$ ratio. $ScAlO^+$ is equivalent to 0.004 ppm Sr for every 1 ppm Sc. $^{40}Ca^{48}Ti^+$ is also a likely interference and the $CaTi^+/Ca^+$ ratio has been estimated from perovskite. The $CaTi^+$ correction represents 8 ppm Sr for every 1 wt% Ti. Molecular interferences account for less than 10% of the m/e = 88 intensity except in GR-1-R hibonite, where the correction is 25%.

6.3.12 $^{89}Y^+$. This isotope has molecular interferences from $CaTi^+$ (see section 6.3.11) and $^{27}Al^{46}Ti^{16}O^+$ (see section 6.3.13) $AlTiO^+$ represents ~4 ppm Y and $CaTi^+$ ~0.9 ppm Y for every 1 wt% Ti. In only one case, that of BB-6 hibonite, did the correction result in an apparently negative abundance. Molecular interferences account for less than 20% of the m/e = 89 count rate except for HAL and BB-6 hibonite.

6.3.13 $^{91,92}Zr^+$. $AlTiO^+$ is a major interference, but its intensity can be calculated using simultaneous equations on intensities recorded at masses 91 and 92. The $AlTiO^+$ and Zr^+ intensities agree well with those calculated using measured count rates at m/e = 93 ($AlTiO^+$ only) and 94 (Zr^+ only). They also agree with $AlTiO^+$ and Zr^+ intensities recorded using simultaneous equations on m/e = 90 and 91 after 90 is corrected for $CaTi^+$.

Concentrations were determined in corundum assuming that, under the same operating conditions, the ion yields are identical to those of hibonite.